A Volcano Rekindled: The Renewed Eruption of Mount St. Helens, 2004–2006
Edited by David R. Sherrod, William E. Scott, and Peter H. Stauffer
U.S. Geological Survey Professional Paper 1750, 2008

Chapter 9

Growth of the 2004–2006 Lava-Dome Complex at Mount St. Helens, Washington

By James W. Vallance[1], David J. Schneider[2], and Steve P. Schilling[1]

Abstract

The eruption of Mount St. Helens from 2004 to 2006 has comprised extrusion of solid lava spines whose growth patterns were shaped by a large space south of the 1980–86 dome that was occupied by the unique combination of glacial ice, concealed subglacial slopes, the crater walls, and relics of previous spines. The eruption beginning September 2004 can be divided (as of April 2006) into five phases: (1) pre-dome deformation and phreatic activity, (2) initial extrusion of spines, (3) recumbent spine growth and repeated breakup, (4) southward extrusion across previous dome debris, and (5) normal faulting of the phase 4 dome to form a depression, a shift to westward extrusion and overthrusting of earlier phase 5 products. Overall, steady spine extrusion gradually slowed from 6 m^3/s in November 2004 to 0.6 m^3/s in February 2006.

Thermal camera data show that phase 1 activity included low-temperature thermal features, such as fumaroles, fractures, and ground warming related to rapid uplift, as well as deformation in the south moat of the crater. The relatively cold (<160°C) phreatic eruptions of early October heralded activity at a subglacial vent situated along the south-sloping margin of the 1980–86 dome. Thermal infrared imagery, documenting increased heat flow, presaged phase 2 extrusion of the October 11–15, 2004, lava spine. The thermal images of the extruding spine revealed a hot basal margin and highest temperatures of 600–730°C.

During phase 3, a recumbent whaleback-shaped spine with a low-temperature shroud of fault gouge and a hot, U-shaped basal margin extruded. This spine pushed southward along the bed of the glacier until it encountered the south wall of the 1980 crater, whereupon it broke up, decoupled, and regrew. Continued southward growth of the recumbent spine pushed cold deformed rock, hot dome rubble, and glacier ice eastward at a rate of 2 m/d. In April 2005, breakup of the whaleback and growth of a lava spine across previous dome rubble heralded phase 4 spine thrusting over previous spine remnants. During phase 4, the active spine pushed southward with an increasingly vertical component and increasing incidence of large rockfalls. In late July, the spine decoupled from its source, the vent reorganized, and a new spine began to grow westward at right angles to the previous growth direction, defining phase 5. Dome migration again plowed glacier ice out of the way at a rate of about 2 m/d, this time westward. In early October, the spine buckled near the vent and thrust over the previous one. A massive spine monolith had been constructed by December 2005, and growth of spines with increasingly steep slopes characterized activity through April 2006.

The chief near-surface controls on spine extrusion during 2004–6 have been vent location, relict topographic surfaces from the 1980s, and spine remnants emplaced previously during the present eruption. In contrast, glacier ice has had minimal influence on spine growth. Ice as thick as 150 m has prevented formation of marginal angle-of-repose talus fans but has not provided sufficient resistance to stop spine growth or slow it appreciably. Spines initially emerged along a relict south-facing slope as steep as 40° on the 1980s dome. The open space of the moat between that dome and the crater walls permitted initial southward migration of recumbent spines. An initial spine impinged on the opposing slopes of the crater and stopped; in contrast, recumbent whaleback spines of phase 3 impinged on opposing walls of the crater at oblique angles and rotated eastward before breaking up. Once spine remnants occupied all available open space to the south, spines thrust over previous remnants. Finally, with south and east portions of the moat filled, spine growth proceeded westward. Although Crater Glacier had only a small influence on the growing spines, spine growth affected the glacier dramatically, initially dividing it into two arms and then bulldozing it hundreds of meters, first east and then west, and heaping it more than 100 m higher than its original altitude.

[1] U.S. Geological Survey, 1300 SE Cardinal Court, Vancouver, WA 98683

[2] U.S. Geological Survey, Alaska Volcano Observatory, 4200 University Drive, Anchorage, AK 99508

Introduction

Continuous, steady extrusion of gas-poor, solidified dacitic magma through glacier ice has characterized the 2004–6 eruption of Mount St. Helens. Dome emplacement has been influenced by the geometry of the 1980 crater, an amphitheater ~2 km across, 500 m deep, and open to the north (fig. 1). In the exact middle of the amphitheater, the 1980–86 dome grew to a volume of about 77×10^6 m^3, attaining dimensions of 860 by 1,060 m in plan and reaching a height of 270 m above the flat-floored amphitheater (fig. 1*A*) (Swanson and Holcomb, 1990). By fall 2004, the north-facing aspect and steep walls, prolific annual snowfall, and frequent winter avalanches in the 1980 crater had given rise to a rapidly growing glacier, as thick as 150 m and with a volume of about 80×10^6 m^3, that wrapped the 1980s dome like a U (fig. 1*B*) (Schilling and others, 2004).

During initial volcanic unrest between September 23 and October 10, 2004, uplift and deformation along the southern part of the 1980s dome and glaciated areas to the south formed a welt more than 100 m high. Deformation of the 1980–86 dome, crater-floor debris, and glacier ice south of the 1980–86 dome has continued throughout the eruption. However, during subsequent dome growth, the locus of deformation has shifted southward, then alternately eastward and westward, as actively growing spines plowed old rocks, recently emplaced but inactive spines, and glacier ice out of their way (Dzurisin and others, 2005).

Following unrest that began on September 23, 2004, and culminated with phreatic eruptions 8–12 days later, intrusion and extrusion of solid magma has typified the eruption. The magma is unusually gas poor (Gerlach and others, this volume, chap. 26) and crystal rich (Pallister and others, this volume, chap. 30). Several meters of pulverized, variably sintered rock (Cashman and others, this volume, chap. 19) has commonly coated emergent lava spines, lending them a smooth appearance. Other spines have broken apart to become surrounded by hot talus fans.

Terminology used in this paper is as follows. A single lava dome was extruded at Mount St, Helens from 1980 to 1986 and a second from October 11, 2004, through the time of this writing. Because of their solid-state character, individual extrusions of the current dome-building eruption are termed "spines," not lobes. The term "recumbent" implies that the horizontal component of extrusion is greater than the vertical component. The term "whaleback" describes a form of smooth-surfaced recumbent spine. Several spines include upthrusted deformed rock of previous crumbled spines and older rock from the 1980–86 dome. Such spines are termed "compound" following Blake (1990) and distinguished from individual growing spines, which are typically monolithic rather than rubbly.

Spine morphologies of the current eruption are variants of Blake's (1990) upheaved plugs and peléean domes but do not include the more fluid, low lava domes and coulees. As of April 2006, the growing dome has included seven spines (figs. 2, 3) but no surface flowage features or extruded silicic lava flows. Spine shapes have included steeply inclined fins, broken blocky forms, and whalebacks (fig. 2). Four of the spines have grown recumbently, and five of them have pushed through thick glacial ice.

Thermal infrared imagery, petrography, and seismology all suggest that extrusion of these solid spines occurred at temperatures below the rock's solidus temperature. Rock samples that are porphyritic, microlite rich, and glass poor are consistent with subsolidus eruption (Pallister and others, this volume, chap. 30). Shallow seismic signals that locate within about 1 km of the surface and an absence of deeper signals (Moran and others, this volume, chap. 2; Thelen and others, this volume, chap. 4) suggest a possible viscous-to-solid transition of the magma at that depth. The hottest recorded temperatures of the extruding spines, culled from >10,000

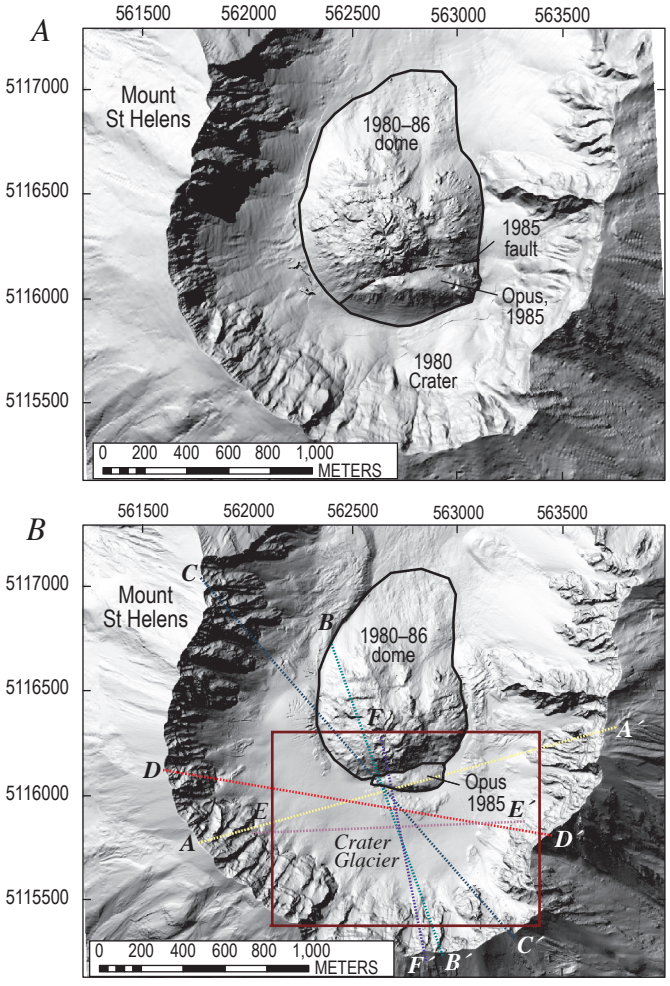

Figure 1. Digital elevation models (DEMs) of Mount St. Helens showing 1980 crater, 1980–86 dome, Opus, and Crater Glacier. Coordinate system is North American Datum 1927 Universal Transverse Mercator, zone 10N, in this and subsequent map figures. *A*, 1986 DEM. *B*, 2003 DEM. Solid rectangle locates DEMs in subsequent figures, and dashed lines locate cross sections illustrated in subsequent figures.

images collected during 37 missions, cluster where cracks and avalanches expose fresh interior surfaces and fall between 700°C and 730°C. These measurements provide a minimum limit for the temperature of extruded spines that is much lower than the solidus temperature of 920–960°C for the dacite of spines 1–7 (Pallister and others, this volume, chap. 30).

The purpose of this report is to document the characteristics of spine growth at Mount St. Helens, the dramatic near-field deformation that accompanied it, and the impact of dome growth on Crater Glacier. To achieve this we examined and analyzed oblique and vertical aerial photography, digital elevation models (DEMs), and thermal infrared imagery. In particular, we used DEMs and aerial photographs to document growth of spines and nearby deformation as a function of time. To illustrate how the dome has grown and how that growth has affected surrounding areas, we generated surface deformation maps and interpretive cross sections. As supporting evidence we considered results reported elsewhere in this volume, such as geologic mapping (Herriott and others, chap. 10), GPS instrumentation (LaHusen and others, chap. 16), and repeat photography from fixed sites (Major and others, chap. 12; Dzursin and others, chap. 14; Poland and others, chap. 11).

Deformation Within the Crater

Methods and Assumptions

During a period of about 18 months, repeated visual observations, oblique aerial photography, thermal infrared imagery, lidar, and high-resolution aerial photography delineated evolution of the 2004–6 dome at Mount St. Helens and deformation of nearby features in response to that growth. Frequent aerial reconnaissance allowed observations and oblique aerial photography as weather permitted. Cascades Volcano Observatory (CVO) staff collected such data almost daily in the period from September 27, 2004, until October 15, 2004. Thereafter, observations were less frequent, with repeat intervals increasing from a few days to as long as eight weeks.

Thermal Infrared Imagery

Thermal infrared (TIR) images allowed estimation of pixel-integrated temperatures for exposed dome-rock surfaces, fumaroles, and other features. More generally TIR surveys showed how surface areas were heated before the appearance of spines at the surface, allowed differentiation of individual spines, showed thermal structures within spines, and revealed how spines evolved and cooled once extruded (fig. 3). We conducted 37 TIR surveys of the deformed area and the growing dome between October 1, 2004, and April 30, 2006.

The instrument used, a FLIR Systems ThermaCAM™ PM595 infrared camera, mounted on a helicopter, is a microbolometer that measures brightness in the 7.5–13 μm waveband to detect temperatures in the range from –40°C to 1,500°C. It collects TIR images as frequently as once per second and can acquire both TIR and standard video (Schneider and others, this volume, chap. 17). Conversions to temperature depend on emissivity, atmospheric temperature, humidity, distance, viewing angle, steam, and gas (Ball and Pinkerton, 2006; Harris and others, 2005). We can independently measure atmospheric temperature, humidity, and distance well enough that resultant errors are about ±10°C; if emissivity is 0.96±0.1, additional errors would be ±5 percent (Schneider and others, this volume, chap. 17). We can only minimize errors owing to the other parameters by repeating measurements at multiple viewing angles and reporting temperature values for conditions with minimal gas and steam. Images from a TIR survey at a distance of about 1 km yield a horizontal field of view of about 210 m and a pixel resolution of about 1.5 m. Integration of brightness within individual pixels means that hottest reported temperatures could be averaged across areas less than 2 m^2 (Schneider and others, this volume, chap. 17).

Repeat Aerial Photographs, Lidar, and DEMs

A sequence of aerial photographs and lidar converted to DEMs provided vertical and planimetric control at intervals of 1 to 55 days during the 18-month study period. Lidar data from November 2003 (Queija and others, 2005) provided initial datum control, and DEMs generated from topographic maps provided control for the 1980 and 1986 surfaces (fig. 1). Three DEMs were derived from lidar surveys made early in the eruption between October 4 and November 20, 2004, (U.S. Geological Survey and National Aeronautics and Space Administration, unpub. data). In addition, Schilling and others (this volume, chap. 8) created 18 DEMs from vertical aerial photography taken between October 4, 2004, and February 9, 2006. The DEMs of October 4 and 13, 2004, (Schilling and others, this volume, chap. 8) provided a check of lidar DEMs collected October 4 and 14.

Identification and Tracking of Features

During the study period, we used aerial photographs and DEMs to identify and track primary and secondary features. Primary features could be located three dimensionally in two or more DEMs and included points at distinctive topographic crests or, less commonly, troughs and intersections of linear features. Examples of point features include distinctive spine formations (for example, fig. 2, point c), megablocks, stranded ice blocks, the toes of avalanches from the 1980 crater walls (fig. 2, points a and i), and seracs. Intersection features include crack networks on the growing dome (fig. 2, point h) and crevasses on Crater Glacier. In many cases, primary features formed of ice and snow persisted only from October 2004 through March 2005. Secondary features are those that we could track approximately in plan view but for which vertical control was difficult or impossible to obtain (fig. 2, features d, e, f, g). Secondary features included margins of actively

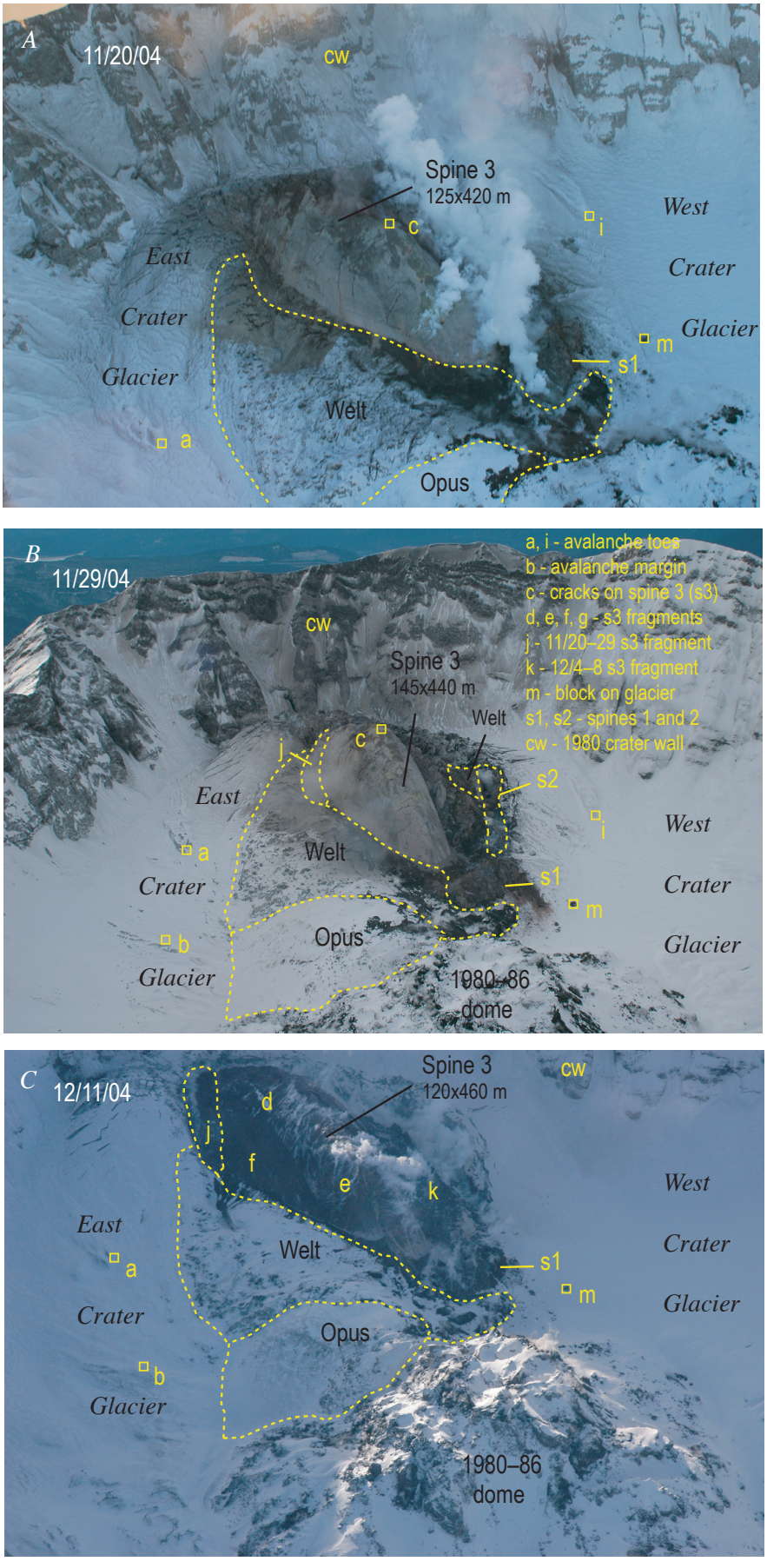

Figure 2. Photographs of Mount St. Helens crater and whaleback-form spines 3 and 4 taken looking south-southwest and illustrating primary and secondary features as they evolved during spine growth and deformation. Features denoted with squares are primary "point" features, and others are secondary features. *A*, November 20, 2004; USGS photo by J.N. Marso. *B*, November 29, 2004; USGS photo by M. Logan. *C*, December 11, 2004; USGS photo by J.S. Pallister. *D*, December 28, 2004; USGS photo by S. Konfal. *E*, January 3, 2005; USGS photo by M. Logan. *F*, January 14, 2005; USGS photo by M. Logan.

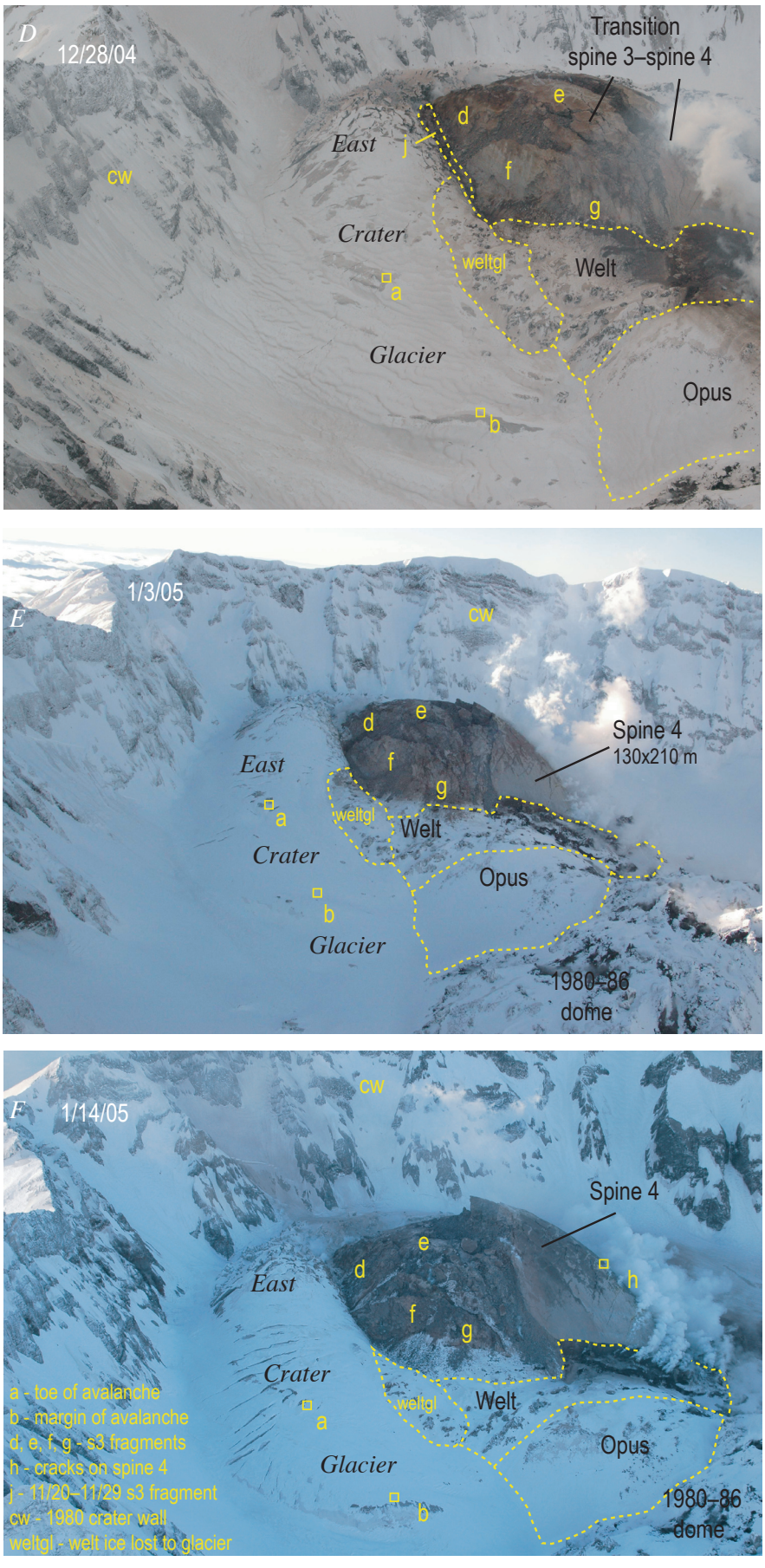

Figure 2—Continued.

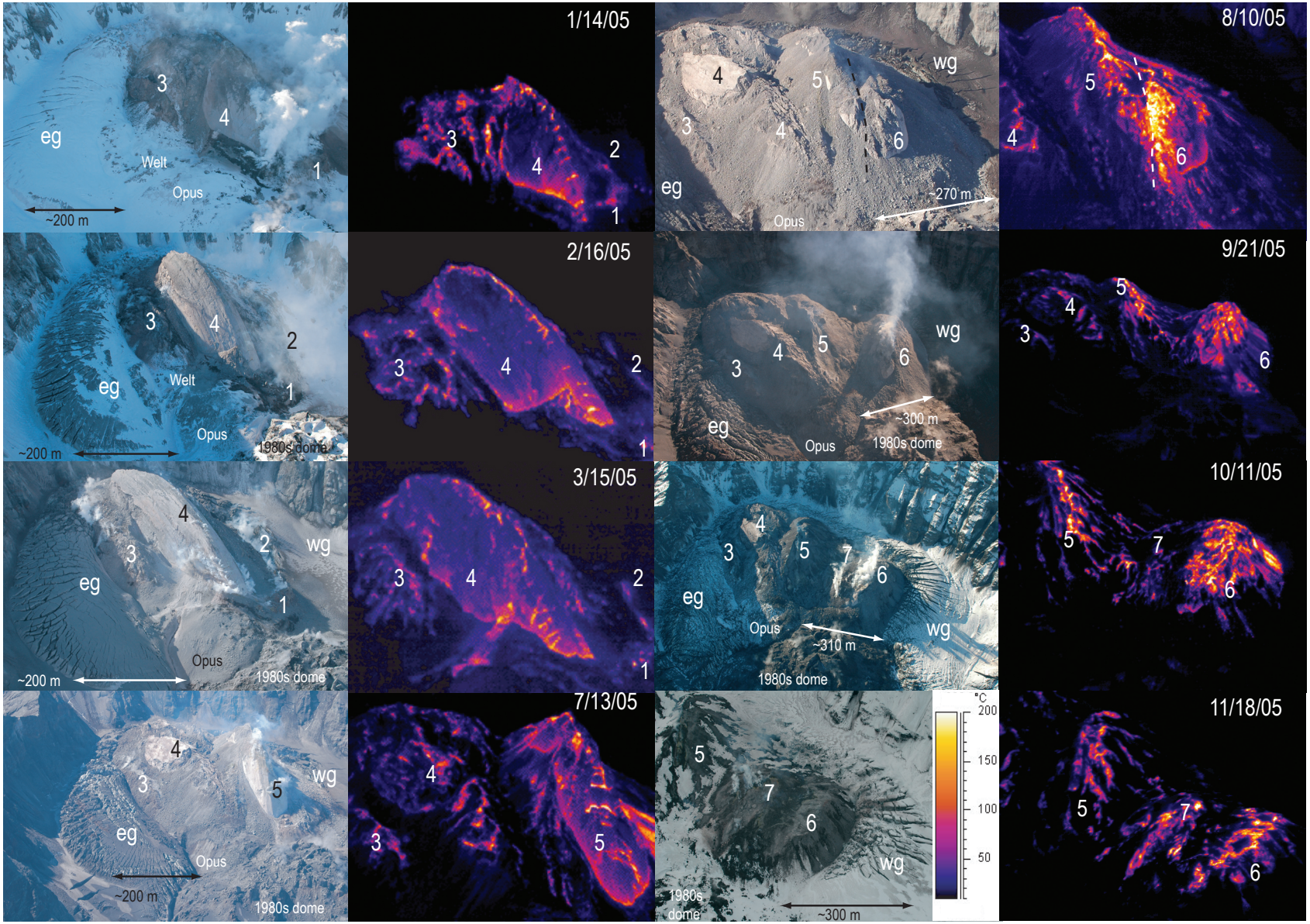

Figure 3. Photograph and thermal-infrared image pairs from Mount St. Helens, views from north-northeast (Jan. 14–Sep. 21, 2005), north (Oct. 11, 2005), and northwest (Nov. 18, 2005), illustrating evolution of the 2004–6 dome. Numbers designate spines 1–7; eg and wg designate east and west Crater Glacier. Dashed line in photograph of Aug. 10, 2005, is trace of fault developing between spines 5 and 6. USGS photos of Jan. 14, March 15, July 11, and Nov. 18, 2005, by J.W. Vallance; those of Feb. 16 and Sep. 21, 2005, by J.W. Ewert; those of Aug. 10 and Oct. 11, 2005, by C.A. Gardner and C. Fox-Lent. Thermal images of Feb. 16 and Sep. 21, 2005, by J.W. Vallance; the remainder by M. Logan.

growing spines, the contact of the 1980–86 dome with the new dome, the contacts of the glacier with the new dome and crater wall, and glacier snouts. Such secondary features provided useful constraints on deformation but could not be used to measure that deformation directly.

Sources of error in locating primary features included accuracy of DEMs, accuracy of repeating a location in a single DEM, identification and location of features in consecutive DEMs, deformation of features with time, melting or addition of snow to features, and misidentification of features in successive DEMs. Precision of DEMs is a few centimeters to about a decimeter (Schilling and others, this volume, chap. 8). On individual DEMs, distinctive features could be relocated to within ±2 m horizontally and ±1 m vertically.

Features were identified and relocated on successive DEMs with some certainty unless the features were obscured by snow, shadows, steam, or clouds or were so deformed during the interval between DEMs as to become difficult to recognize. Fresh snow and ablation may have affected relocation and ultimately even recognition of primary features, but some areas on or near the active dome were windswept or remained warm year-round; features in such areas were not subject to relocation errors related to melting or snowfall. Comparison of relative motion of groups of neighboring objects provided a check on correlations. We eliminated correlations that yielded results greatly at variance with those of neighboring objects.

Generally, error in locating primary features in successive DEMs is between ±2 m and ±5 m in the horizontal and vertical dimensions. Features subject to the most deformation—those on or near the actively growing dome—tend to be those with the greatest errors in relocation. Features away from the locus of deformation may have small absolute location errors but may not move far enough to register significant motion, given the magnitude of error in locating them.

Generation of Surface-Deformation Vectors

Primary features that can be located in two or more successive DEMs allow estimation of vector components from one time to another. This allows calculation of average rates of deformation (for example, points a, b, c, and h in fig. 2). As we know of no systematic source of error in locating primary features, errors should not tend to accumulate for features that can be located in three or more successive DEMs. Repeated locations of primary features indicated in figures by solid arrows thus allow generation of surface-deformation vectors within our stated error limits.

Successive locations of secondary features give a sense of magnitude and direction of deformation but do not yield true vectors. In such cases, the vertical component of deformation may be poorly known or unknown. Despite poor constraints on vertical position, plan-view locations of some secondary features are as accurate as those of primary features. Examples include features located in rectified aerial photographs for which no DEM exists and features that crumble as they move laterally yet still can be identified. Crumbling features are common on or near active spines. Relocations of such features can be accurate in plan; but vertical changes, if given, are minimum values. Relocations of secondary features such as the contact between the glacier and active dome give minimum constraints on deformation in both horizontal and vertical directions.

Vector Fields

Vector fields were derived from simultaneous tracking of numerous primary features on successive DEMs. Vector fields were used to delineate growth of active spines, deformation of inactive parts of the dome and its surroundings, and deformation of the glacier in locations where motion exceeded a threshold of about 4 m in the time between successive DEMs. Because DEMs were produced at intervals of 9–55 days and vertical and horizontal precision were ~5 m, detection limits for time-averaged deformation rates range from 0.6 to 0.09 m/d.

Comparison with GPS Data

During certain intervals, portable GPS receivers that provided nearly continuous measurement of deformation (LaHusen and others, this volume, chap. 16) were located near features tracked during this study using DEMs, thereby providing a check on our results. The GPS deformation measurements compared well with those of this study. For example, a GPS receiver placed on the spine during November 21–29, 2004, gave a vector almost identical in magnitude and direction (10.3 m/d, S. 19° E., up 6°) to that of a nearby feature 30 m east that we tracked November 20–29 (10.4 m/d, S. 21° E., up 8°).

Our deformation measurements have advantages and disadvantages compared with those derived from GPS receivers. The chief advantage of our approach is that we can track numerous features simultaneously and thus obtain a complete picture of dome growth and nearby deformation patterns. GPS sensors are advantageous in that their data streams can be sampled frequently and transmitted back to the observatory. Such real-time acquisition permits the use of GPS data in monitoring. In contrast, our measurements are values averaged over intervals between successive DEMs and have no application in real-time monitoring because of the additional time required to prepare DEMs.

Volume and Flux Calculations

All reported volumes assume the 1986 topographic surface as a datum and subtract it from DEMs of various dates over pertinent areas (hot-rock volumes given in Schilling and others, this volume, chap. 8). Because thick glacial ice overlay the 1986 debris fill of the moat by 2004, we chose the 1986 surface as a datum for volume calculations rather than the more recent ice-mantled surface of 2003–4. To facilitate calculations, we assumed that bounding surfaces between the datum and the areal extent of hot rock on any subsequent DEM were

vertical. The assumption of vertical bounding surfaces dictates that calculated volumes are minimum values in cases where natural surfaces differ substantially from vertical. A steep, near-vertical contact between the extruding dome and glacier ice is probably a reasonable assumption for two reasons. First, visible upper parts of glacier contacts with hot rock were steep and nearly vertical. Second, relict ice-hot rock contacts exposed in other volcanic areas are commonly nearly vertical because the ice cools and buttresses the rock margin, preventing avalanches and rockfall that tend to form slopes more closely approaching the angle of repose.

Time-averaged volumetric extrusion rates for individual spines are derived by comparing volumes from one DEM to the next and dividing by the time between them. In many cases, volumetric rates are the same as the hot-rock extrusion rates of Schilling and others (this volume, chap. 8). Well-constrained growth intervals of certain spines allow more precise calculation of their volumetric extrusion rates.

Cross Sections

Cross sections were constructed from DEMs sampled at horizontal intervals of 10 m, are presented with no vertical exaggeration, and include both simple representations of successive surfaces and interpretive relations among units at depth. Our guiding philosophy in the construction of cross sections was not to extend geologic interpretation below levels for which we have no constraints. Therefore none is extended below our lowermost control surface, that of summer 1980.

Phases of Dome Growth at Mount St. Helens

Between the onset of unrest on September 23, 2004, and April 2006, the eruption developed in a manner that is divisible into five distinct phases, each with characteristic rate and pattern of eruption (table 1). An initial brief vent-clearing phase included seismic unrest, spectacular deformation features, and phreatic explosions developed in the moat between the 1980s dome and the 1980 crater walls. Initial spine extrusion began October 11, 2004. As extrusion continued, the locus of spine growth shifted, spines grew and stagnated, and new ones formed in their stead (table 1). As of April 2006, a total of seven discrete spines have erupted that we have grouped on the basis of similar growth patterns into four additional phases (table 1).

Phase 1, Precursory Vent Clearing, September 23–October 10, 2004: Phreatic Explosions and Deformation

The first indications of an impending eruption included a week of intensifying seismicity beginning September 23, 2004, deformation-induced surficial cracks in glacier ice south of the 1980–86 dome that began to appear by September 29 (Dzursin and others, this volume, chap. 14), and four phreatic explosions between October 1 and 5 (Moran and others, this volume, chap. 6). The phreatic explosions formed a vent at the west edge of deformed ice. Thermal IR images show that the explosions of early October had temperatures of no more than 160°C (Schneider and others, this volume, chap. 17). On the basis of these low temperatures, we infer that the explosions were phreatic rather than magmatic. However, the explosions did indicate interaction of hot rock with the shallow hydrothermal system, thus suggesting rise of magma to near the surface.

During early October, a zone of highly fractured ice developed and expanded southward as subsurface intrusion fractured and thrust the part of the 1980–86 dome called Opus, which had formed in 1985, and adjacent crater-floor debris upward to form a feature named “the welt” (fig. 4). This shallow intrusion of magma caused surface uplift in excess of 70 m (figs. 5, 6). Uplift was greatest along a north-south axis about 200 m east of the October vent (fig. 5) and diminished rapidly away from that axis.

The welt expanded southward, but motion of recognizable features through October 4 was upward and northward along a reverse fault with a strike of ~N. 80° E. and located between Opus and the remainder of the 1980–86 dome to the north (fig. 5). This faulting apparently reactivated a normal fault of 1985 that bounded the north margin of the Opus feature (fig. 1*A*). Surface deformation vectors south of the fault trace show motion of 25–30 m north and 50–70 m up. If deformation indicated motion along the fault, then its dip was ~60° south.

During October 4–14 the locus of deformation migrated south from Opus, and the sense of motion at the surface was radial, away from the most intense deformation. Motion on Opus was undetectable to barely detectable at ~5 m east and up (figs. 5, 6). On glacier surfaces, ballistic impact sites and distinctive avalanche toes near the periphery of the welt moved 5–15 m away from the welt (southwest to east) and up (fig. 5). The few traceable points on the eastern and central parts of the actively deforming welt moved 30–80 m eastward away from the axis of the welt (fig. 5).

The DEMs of October 13 and 14 recorded displacement in the range of 5–30 m along the surface of the expanding welt (fig. 5). Points along the deformation axis, which coincided with the axis of spine 3 when it later emerged in November, moved 15–30 m S. 10° E. along the axis and rose 6–8 m in one day. Nearby features to the east moved laterally 12–15 m S. 20° E. to S. 45° E., with little vertical motion. Features on fractured ice to the east also moved away from the growing welt, whereas those on Opus showed no detectable motion.

Phase 2, October 11–24, 2004: Spines 1 and 2

Initial Spine Growth

Spines 1 and 2 each extruded rapidly within a few days and thereafter remained inactive, though each was affected

Table 1. Timing, extrusion rates, character of dome growth, deformation within crater, and impact on glacier during each of five eruptive phases from September 2004 to April 2006, Mount St. Helens, Washington.

[Estimates of extrusion rates are derived from comparing DEMs from one date to the next (Schilling and others, this volume, chap. 8; and this chapter). Estimates of linear advance are obtained from tracking features in DEMs or aerial photographs (this chapter), from repeat photos from fixed positions (Major and others, this volume, chap. 12), and from portable GPS stations (LaHusen and others, this volume, chap. 16).]

Phase	Spine	Time period	Growth rate	Nature of eruptive activity	Deformation within 1980 crater	Effect on glacier
1—Precursory vent clearing	Pre-dome	Sept. 23 –Oct. 10, 2004	Not applicable	Vent clearing and phreatic explosions. Ascent of solid spine to surface.	Uplift of 1980–86 dome, and crater floor to north of 1980–86 dome to form welt. By Oct. 4, 2004, total volume of deformed area (welt) is ~5×10^6 m^3.	Disruption and uplift of Crater Glacier.
2—Initial spines	Spine 1	Oct. 11–15, 2004	2–3 m^3/s; 15–20 m/d	Near-vertical spine growth.	Continuing uplift of crater floor to south of 1980s dome; Volume of deformed welt increases, 5×10^6–11×10^6 m^3, Oct. 4–13, 2004.	Continuing uplift and disruption of glacier but no appreciable melting.
	Spine 2	Oct. 15– ~Oct. 24, 2004	3 m^3/s; 25 m/d	Advance of spine 2 to the south; probable subterranean and subglacial intrusion of spine 3.	Locus of deformation shifts southward and eastward; formation of roof pendant over intruding spine.	
3—Recumbent growth of whaleback spines	Spine 3	Oct. 25– Dec. 18, 2004	4–6 m^3/s; 8–11 m/d	Recumbent growth of spine 3 toward south crater wall; spine 3 begins pushing against south crater wall ~Nov. 12, 2004.	Emerging spine displaces older rocks to east and south; roof pendant is transported to south end of spine 3; spine 2 subsides.	Growth of spine 3 divides Crater Glacier into east and west arms. Spines 3 and 4 plow east Crater Glacier eastward and thereby thicken it as much as 100 m; crevasses form parallel to maximum principal-strain direction (~east–west) but no appreciable melting.
	Transition	Dec. 18, 2004–Jan. 3, 2005	No data	Spine 3 deflects off south crater wall, fractures, breaks up, and decouples from source.		
	Spine 4	Jan. 3–Apr. 9, 2005	1.5–2.5 m^3/s; 5–8 m/d	Continuing extrusion forms spine 4, which continues pushing to the south.	Southward growth of spine 4 tilts and pushes spine 3 to east; deformed 1980–86 debris migrates eastward; remnants of spines 1–3 to west are static	
4—Spine thrusts over previous spines	Transition	Apr. 10–19, 2005	No data	Spine 4 encounters south crater wall, fractures, and decouples from source.		East Crater Glacier deformation slows, then stops; glacier responds to thickening caused by previous deformation by accelerating downslope to north. West Crater Glacier is pushed west.
	Spine 5	Apr. 19-July 18, 2005	1–1.5 m^3/s; 3–6 m/d	Spine 5 thrusts over spine remnants west of spine 4. Smooth surface forms at north end of spine and gradually steepens. In June, spine fractures to the south and disintegrates.	Deformation to east is greatest near vent and diminishes south. This deformation slows and stops. Deformation to west is moderate and continual. Rockfall from spine 5 buries spine 2, then 1.	
		July 19–31, 2005		Spine 5 crumbles to feed rockfall avalanches and slumping events.		
5—Spines grow to west, then thrust over one another	Transition	Aug. 1–5, 2005	No data	Spine 5 fractures near its source and begins to slump.		West Crater Glacier thickens and cracks owing to westward migration of spines 6 and 7; cracks radiate westward along maximum principal-strain axes.
	Spine 6	Aug. 6– Oct. 9, 2005	1.5–2 m^3/s; 3–4 m/d	Sag depression grows owing to slumping of spine 5 and westward migration of spine 6; spine growth is chiefly recumbent and endogenous.	Deformation to west; east part of 2004–5 dome complex is stagnant.	
	Spine 7	Oct. 9, 2005 –Apr. 2006	0.5–1 m^3/s; 1–2 m/d	Endogenous growth followed by exogenous spine growth in depression.	Spine 7 pushes spine 6 to west and begins thrusting over elements both of itself and of spine 6.	

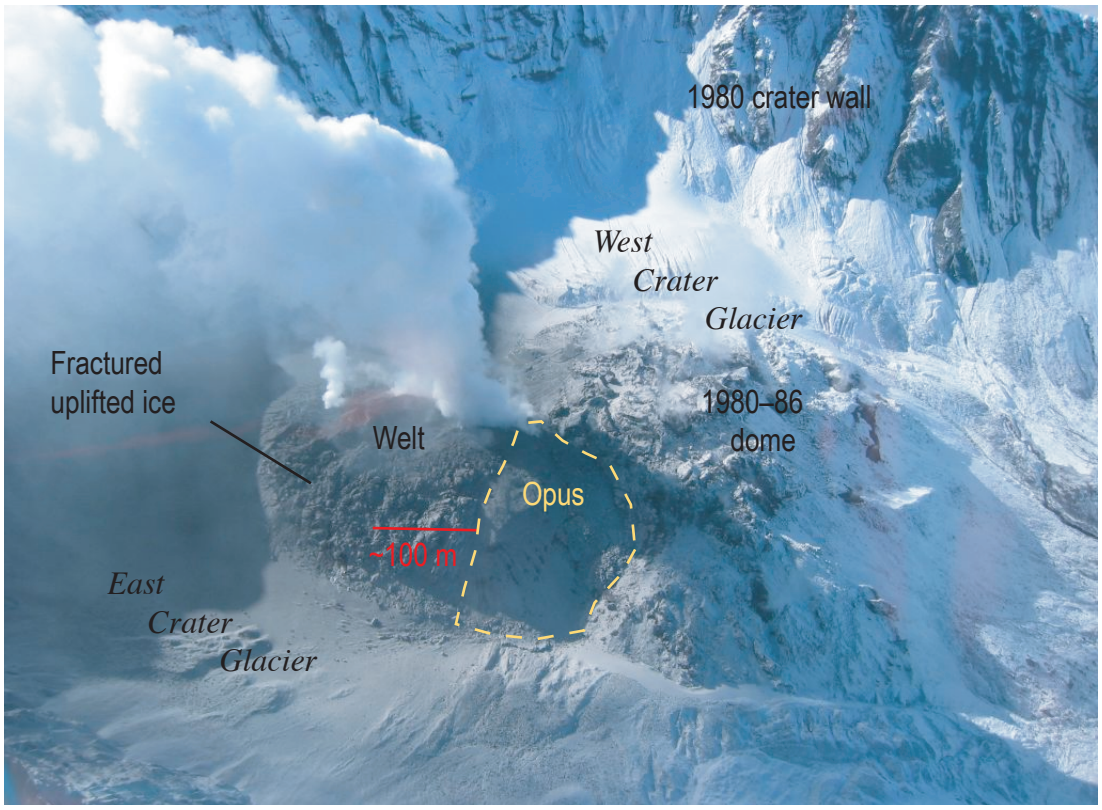

Figure 4. View of Mount St. Helens crater from north-northeast on October 10, 2004, illustrating welt, Opus, 1980–86 dome, crater wall, and Crater Glacier. USGS photo by R. Wessels.

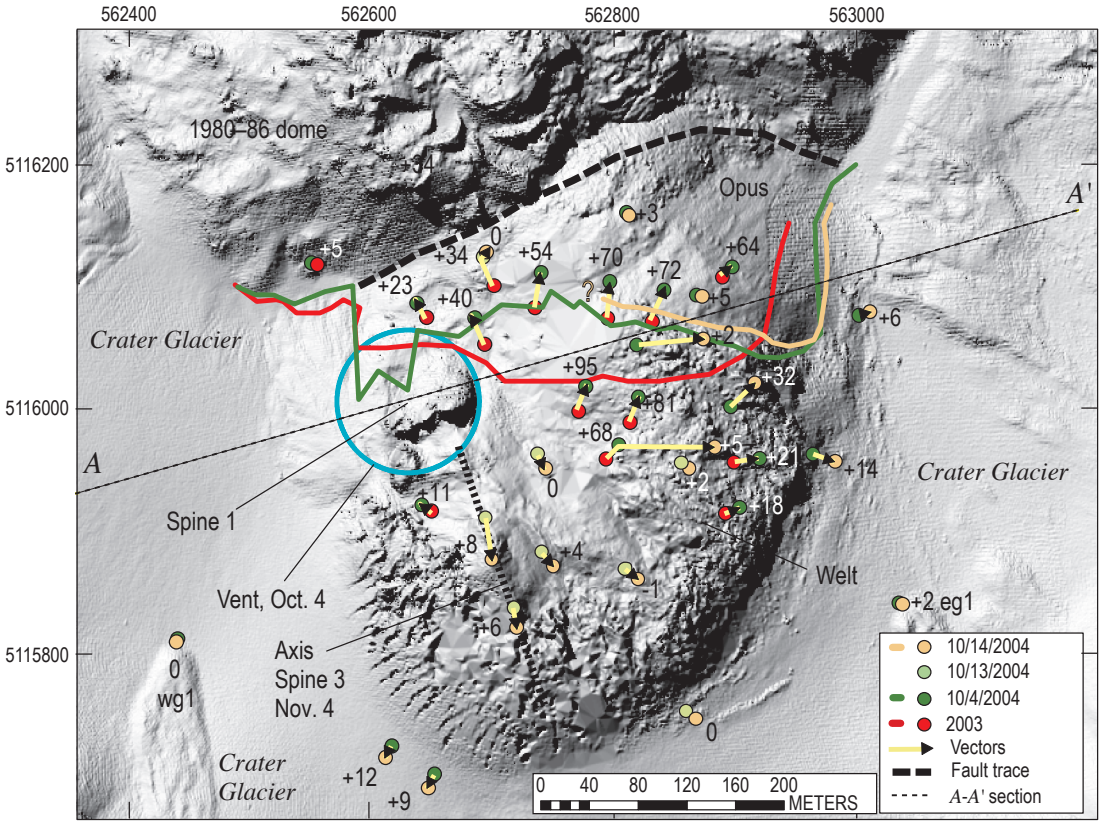

Figure 5. DEM of October 14, 2004, locating vent of October 4, 2004, and illustrating initial extrusion of spine 1 and locations of welt, Opus, 1980–86 dome, Crater Glacier, and cross section *A*–*A*´ shown in figure 6. Dots indicate features tracked, and solid lines indicate changes in fractured ice margin for dates identified by color in key. Arrows show surface deformation vectors; numbers show vertical component of vectors in meters.

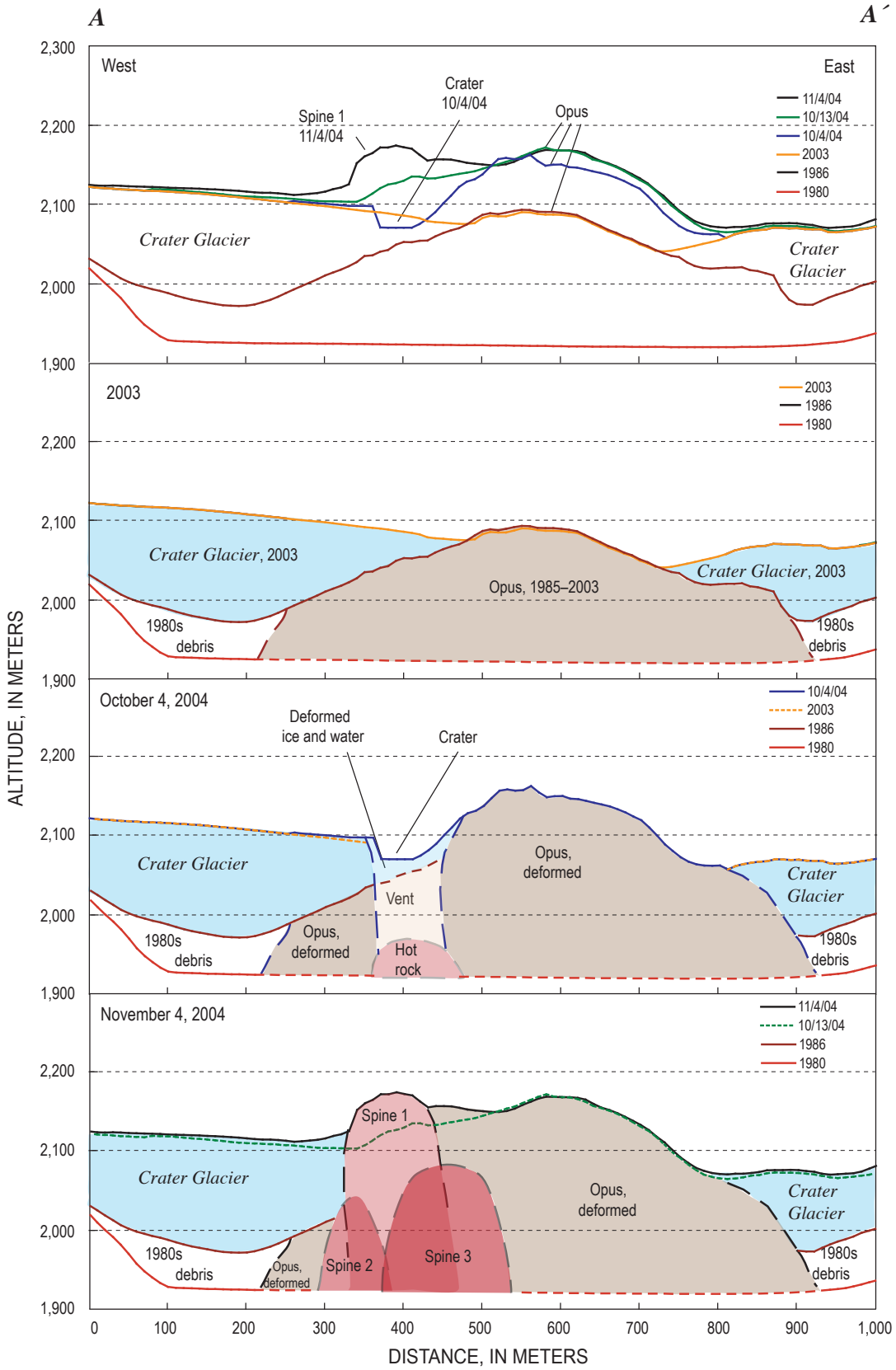

Figure 6. Cross section *A*–*A´* (location shown in figure 5) illustrating extrusion of spine 1, intrusion of spines 2 and 3, and deformation of Opus and glacial ice. Top panel shows known profiles for the dates given, and other panels illustrate geologic interpretations on given dates.

subsequently by deformation and eventual burial. Warming at the surface of the welt to as much as 50°C on October 10, 2004, presaged the appearance of juvenile rock above ground on October 11 (Schneider and others, this volume, chap. 17). Spine 1 extruded from October 11 to 15. Owing to poor weather, the timing of spine 2 emplacement is less well constrained. Observations and study of oblique photographs showed that its growth began after October 15 and finished by October 24.

Spine 1 grew at a steep angle as a solid blocky slab from a south-facing slope on the west part of Opus. By October 14, it was 85×60 m, ~60 m high, dipping 50° northwest, and had volume of ~0.6×10^6 m^3 (table 2, fig. 6). Using the outline of spine 1 on the DEM of November 4, we calculate that the total volume of spine 1 was then ~0.9×10^6 m^3. Spine 1 extruded rapidly, 15–20 m/d and 2–3 m^3/s (table 2).

Although observations between October 15 and 24 were insufficient to delineate the nature of spine 2's growth directly, it emerged just south of spine 1 and appeared at the surface from north to south as though the deformed glacier ice from which it emerged had unzipped rapidly southward. It emanated from the October 4 vent (figs. 5, 7) and moved southward along subglacial slopes to form an elongate body oriented north–south at the surface (table 2). Its growth ceased when it encountered steep opposing slopes of the 1980 crater. Assuming vertical boundaries downward from the November 4 surface to the 1986 surface allows a volume calculation of about 2×10^6 m^3. The spine's estimated volume and interval of emplacement imply a time-averaged extrusion rate of ~3 m^3/s.

Deformation Accompanying Spine Growth

Between October 14 and November 4, the locus of maximum deformation propagated south along an axis oriented ~S. 20° W. Deformation diminished with distance normal to this axis. Opus and the 1980–86 dome were essentially static during this period (fig. 7). Severely deformed ice on the welt just east of its axis moved a few meters to the north; farther south, it moved as much as 60 m to the southeast and subsided (fig. 7). On glacier surfaces to the east, distinctive features moved 5–40 m eastward and rose 5–20 m. Farther north, glacial features moved a few meters northward. The few traceable points on ice west of the actively deforming welt rose a few meters, but only one feature nearest the northwest margin of the welt moved significantly westward, by ~10 m (fig. 7, point wg1).

Phase 3, Recumbent Growth of Spines 3 and 4: October 24, 2004–April 9, 2005

Growth of Whaleback Spine 3: October 24–December 18, 2004

During mid-October, spine 3 began intrusive growth and pushed into pre-2004 rock, deforming the welt, disrupting glacier ice, and forming a cryptodome beneath the welt (fig. 8). Evidence in support of intrusion included (1) deformation along an axis S. 19° E. that coincided with the axis of spine 3 when it later emerged (fig. 5), (2) upward and southward motion of pre-2004 rock along a trend similar to that of the whaleback when it emerged (figs. 5, 7), and (3) warming of rock at the surface near the axis of deformation (Schneider and others, this volume, chap. 17).

Spine 3 breached the deformed surface of the welt and advanced rapidly to the south-southeast between late October and mid-December to form a smooth-surfaced whaleback feature 300–460 m long and 120–145 m wide (tables 1, 2). Between October 24 and 27, spine 3 emerged from an area about 50 m southeast of spine 1, through older dome and crater-floor rock along the crest of the deforming welt (fig. 9). By early November, it was 320×125 m, with a long axis oriented S. 18° E. (fig. 7). As the spine pushed southward from mid-November through December, its long axis pivoted 9° eastward (to S. 27° E.) about its origin at the vent (table 2).

The surface of the whaleback had a cool and smooth, but striated, surface except on the west, where it was broken and blocky. The striations at the surface of the whaleback were interpreted as slickensides (fig. 10). Growth of the whaleback also lifted a partial roof composed of fractured 1980–86 dome rock and crater-floor debris and transported it southward during November 4–29 (fig. 10). Cashman and others (this volume, chap. 19) show that the smooth outer carapace of the whaleback comprised powdered, partially sintered 2004 dacite plus small amounts of 1980–86 dacite; they interpret this material as fault gouge formed through comminution as the solid spine rubbed and ground against older rock during its ascent in the conduit.

The stable crust of spine 3 insulated the hot rock within so that surface temperatures were low. Thermal images commonly showed a ~200°C zone around the base of the emerging spine (fig. 11*A*), and hot cracks showed rock temperatures as high as 730°C. The temperature of smooth, uncracked parts of the surface diminished exponentially with distance from the source at the base of the spine and approached ambient within 50 m (fig. 11*B*). Because the temperature also decreased exponentially with time (each 10 m from source represented about a day), the moving surface of the spine showed a classic Fourier's Law decline in temperature (Turcotte and Schubert, 1982). Such a temperature profile resembles those observed for blocky lavas at Santiaguito, Guatemala (Harris and others, 2002, 2004), though the lava core temperatures of Mount St. Helens spines differ from those of lavas at Santiaguito in likely being 100°C or more below solidus temperature.

Subtracting the spine 1 and 2 volumes from the total volume of hot rock emplaced by spines 1, 2, and 3 (Schilling and others, this volume, chap. 8) yields values for spine 3 volume and for its extrusion rate between late October 2004 and early January 2005 (table 2). Extrusion rate (flux through the 1986 surface) was ~5 m^3/s until November 4. Extrusion rates then declined from 4.4 to 2.5 m^3/s between late November and early January (table 2).

Table 2. Dimensions, orientation, volume, and growth rate of the welt and spines of Mount St. Helens, Washington, at various dates.

[Applicable interval for linear and volumetric growth rates and direction is from date of previous DEM to date of DEM given for row, unless specifically indicated.]

Phase	Date of DEM	Spine/ Welt	Dimensions (m)	Orientation of welt or spine	Linear growth rate, direction, period of interest, and GPS station name where applicable	Volume ($\times 10^6$ m^3)	Volumetric growth rate (m^3/s)
1—Precursory vent clearing	Oct. 4, 2004	Welt	370×370	Equant	~70 m/d, South, Sept. 29–Oct. 4	5 [a]	12 Sept. 29–Oct. 4
	Oct. 14, 2004	Welt	470×380	Long axis north-south	~10 m/d, South, Oct. 4–14	11 [a]	7
2—Initial spines	Oct. 14, 2004	Spine 1	85×60	Strikes S55W; dips 50° NW	15-20 m/d, S35E, Oct. 11–14	0.6	~2 Oct. 11–14
	Nov. 4, 2004	Spine 1	150×45	Strikes S58W; dips 80° NW		0.9	~3 Oct. 14–15
		Spine 2	240×50	Long axis, Due S	~25 m/d, South, Oct. 15–24	2	3 Oct. 15–24
3—Recumbent growth of whaleback spines	Nov. 4, 2004	Spine 3	320×125	Long axis S18E; dip at vent 30°	11.4 m/d, ~ S5W, Nov. 4–7	9	4.7 Oct. 13–Nov. 4
	Nov. 20, 2004	Spine 3	420×125	Long axis S19E	11 m/d, S22E, Nov. 4–20		
	Nov. 29, 2004	Spine 3	440×145	Long axis S23E	10.3 m/d, S19E, Nov. 21–29, ELEA [b] 10.5 m/d, S21E, Nov. 20–29	18	4.4 [a] Nov. 4–29
	Dec. 11, 2004	Spine 3	460×120	Long axis S27E	7–8 m/d, ~S20E [c]	23	4.1 [a]
	Jan. 3, 2005	Spine 4	210×130	Long axis S27E	4–7 m/d, ~S20E [c]	5.5	2.5 [a]
	Feb. 1, 2005	Spine 4	340×145	Long axis S28E	8.3 m/d, S19E, Jan. 15–16, CDAN [b]	10	1.8 [a]
	Feb. 21, 2005	Spine 4	400×150	Long axis S31E	5.8 m/d, S30E, Feb. 8–14, AHAD [b] 4.5 m/d, S32E, Feb. 1–21	14	2.4 [a]
	Mar. 10, 2005	Spine 4	440×140	Long axis S35E	3.9 m/d, S39E, Feb. 21–Mar. 10	17	1.8 [a]
	Apr. 19, 2005	Spine 4	490×140	Long axis S40E	2.6 m/d, S71E, Mar. 10–Apr. 19 Spine 4 decouples from vent during this interval.	21	1.5 [a]
4—Spine thrusts over previous spines	Apr. 19, 2005	Spine 5	100×90	Long axis S25E; dip at vent 40°	3.5–4.5 m/d, S10E [c]	1	1.5 [a]
	June 15, 2005	Spine 5	340×170	Long axis S9E	3–4 m/d, S along axis [c]	8	1.4 [a]
	July 14, 2005	Spine 5	285×105	Long axis; S5E; dip at vent 54°	2–3.5 m/d, S along axis [c]	11	1.3 [a]
	Aug. 10, 2005	Spine 5				15	
5—Spines grow to west then thrust over one another	Aug. 10, 2005	Spine 6	100×90	Long axis S43W	3–4 m/d, ~West [c]	1; compound spine 6 is ~12	2.0 [a]
	Sept. 20, 2005	Spine 6	350×280	Long axis S47W	3–4 m/d, ~West [c]	6; compound spine 6 is ~17	1.6 [a]
	Oct. 24, 2005	Spine 7	110×40	Long axis S44W	3–4 m/d, ~West [c]	New lava, spines 6+7, ~9	0.9 [a]
	Dec. 15, 2005	Spine 7	260×~250	Long axis S74W	~3 m/d, ~West [c]	New lava, spines 6+7, ~12	0.7 [a]
	Feb. 9, 2006	Spine 7	310×~300	Long axis S83W; dip at vent 50°	2.2 m/d, S80W, up 50°	New lava, spines 6+7, ~15	0.6

[a] Schilling and others (this volume, chap. 8).

[b] LaHusen and others (this volume, chap. 16).

[c] Major and others (this volume, chap. 12).

Growth of Spine 3: Onset of Recumbent Growth

Although the spine in early November 2004 appeared to grow more or less vertically from the axis of the welt, it in fact originated from a source beneath spine 1 and extended southward two to three times as fast as it pushed upward. Between November 4 and 7, identifiable features on the spine's surface moved ~32 m S. 5° W. (fig. 10). Vertical movement of the spine was poorly constrained but appeared to be ~12 m up. The south end of the spine extended almost 30 m S. 19° E., an orientation matching that of its long axis. A possible explanation for the contrast in surface-vector directions and overall spine extension is that, at this early stage of its growth, the spine rotated slightly westward while pushing south-southeast along its axis.

Deformation Adjacent to Spine 3 in Early November

Between November 4 and 7, areas to the east of spine 3 moved tens of meters parallel to the spine or were pushed in easterly directions, and areas to the west and north of spine 3 moved less than 10 m or remained static. Rock debris adjacent to the eastern margin of spine 3 moved parallel to the east margin by almost 30 m (fig. 10*A*). Rock debris farther east moved smaller distances. Motion of the rock debris had no detectable vertical component. Fractured and previously uplifted glacial ice less than 200 m east of the spine moved 10–15 m along trends ranging from southeast to east (fig. 10*A*). During November 4–7, a GPS unit west of the whaleback, CLF4, moved 8 m south-southwest and subsided 2 m

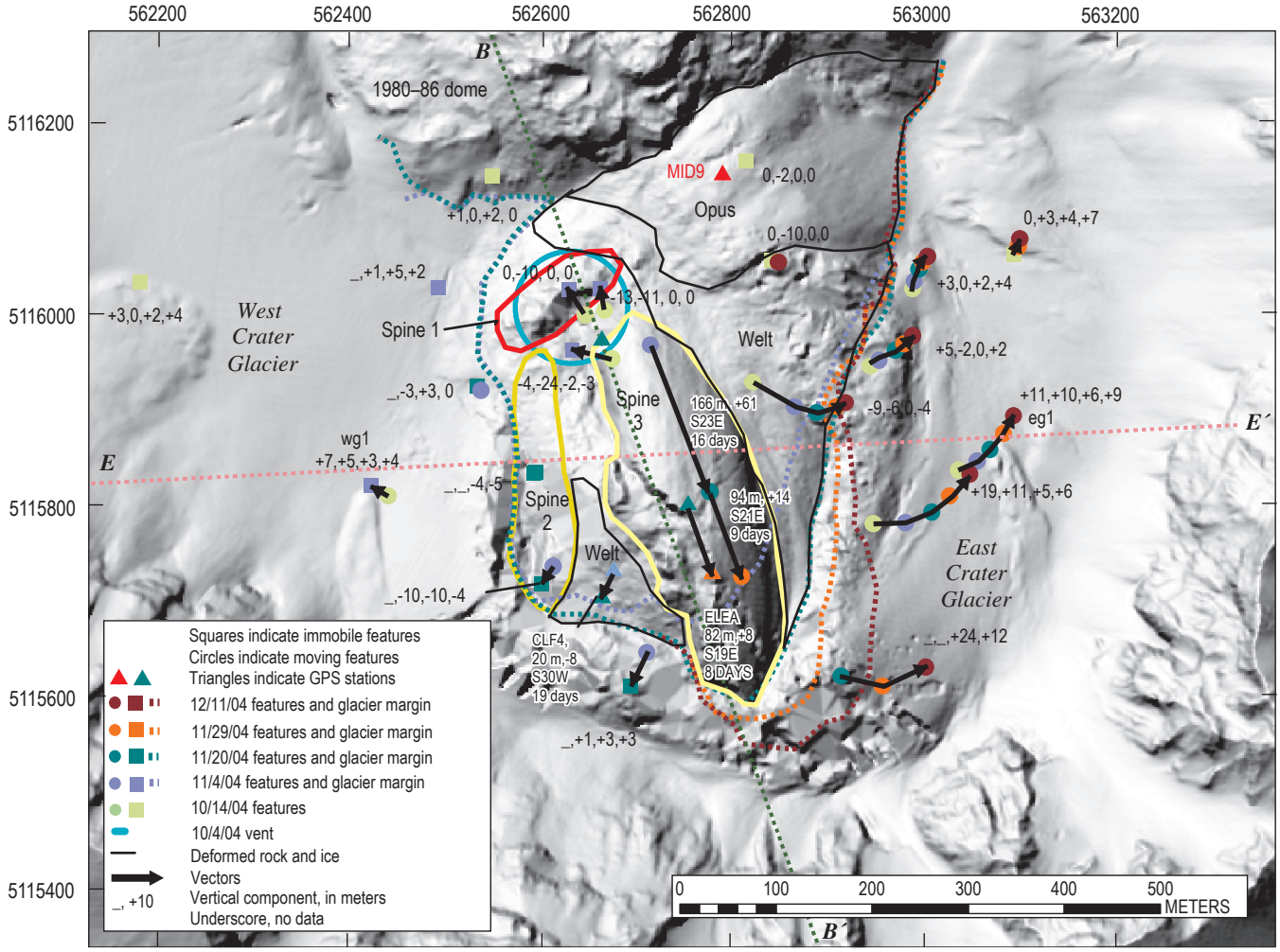

Figure 7. Deformation vectors for the period October 14–December 11, 2004, shown on DEM of November 20. Squares and dots indicate features tracked for dates identified by color in key. These colored symbols delimit deformation vectors of each of the four time intervals between relocation of features. For quantitative data (example: _, -3, +3, 0), numbers are vertical components of vectors, in meters, for each interval. Underscores indicate no data for that interval. Dotted lines indicate dome-glacier margins for dates indicated by color in key. Lines ***B–B´*** and ***E–E´*** are traces of cross sections shown in figures 8 and 14, respectively.

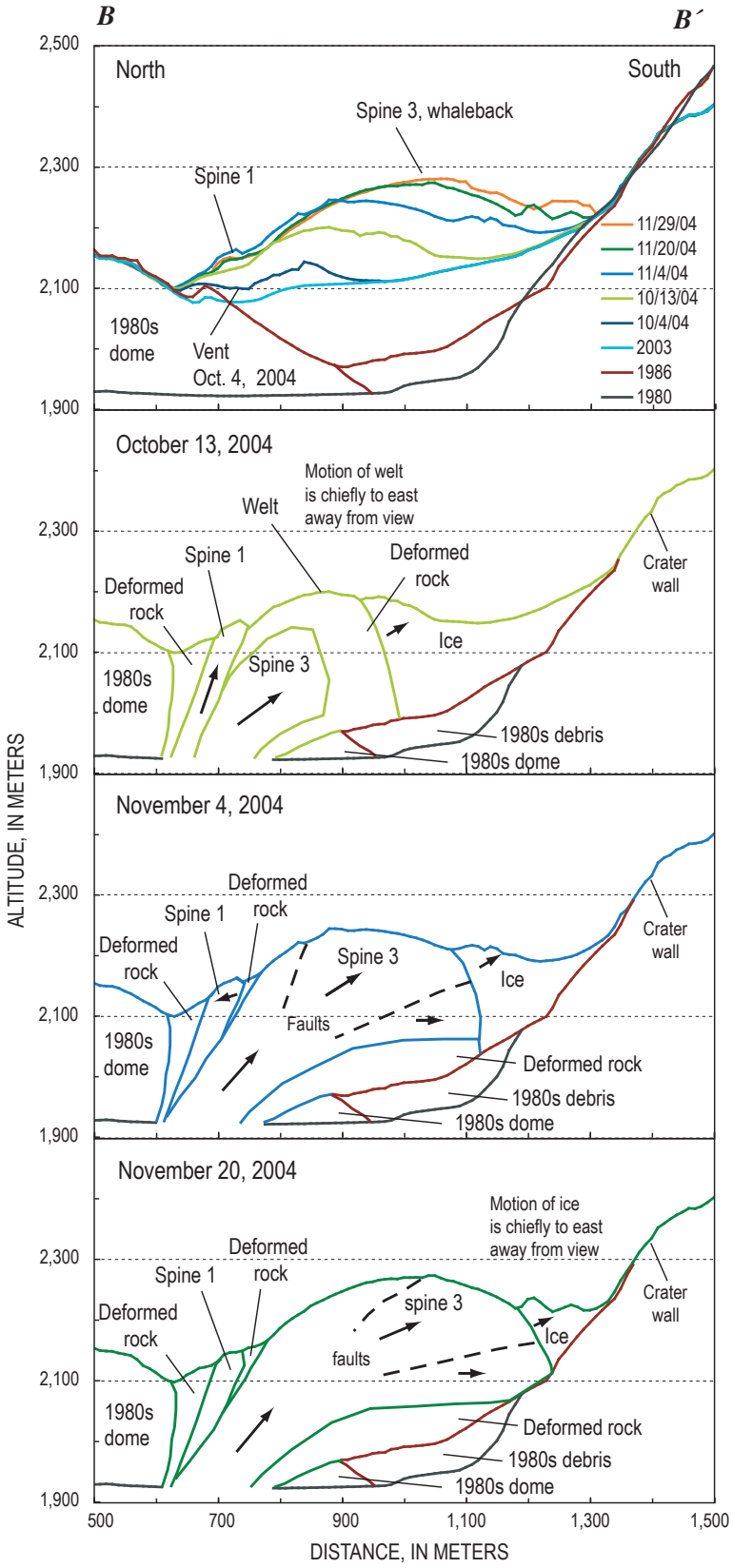

Figure 8. North-south cross section ***B–B´*** (location shown in figure 7) illustrating intrusion and recumbent growth of spine 3. Top panel shows known profiles for the dates given, and other panels illustrate geologic interpretations on given dates.

(LaHusen and others, this volume, chap. 16). Nearly static areas during this time included spines 1 and 2, Opus, and the west arm of Crater Glacier.

Striations and Relative Motion of Spine 3 in Early November

Growth of spine 3 and nearby deformation patterns explain otherwise enigmatic bidirectional striation patterns on the spine in early November 2004. On November 4, 7, and 10, striations plunging 31° N. 66° E. on the east face of spine 3 were superimposed on fainter striations plunging 20° N. 5° E. (fig. 10*B*). At the north end of the spine near the vent, only fainter N. 5° E. striations existed. A cursory analysis in early November suggested that the striations recorded a change in direction of spine growth, with the fresh striations indicating the most recent direction. However, our photogrammetric analysis indicates instead that welt debris adjacent to the whaleback was being dragged at a rate of almost 10 m/d along the base of the emerging spine along a ~S. 32° E. trend (fig. 10). This vector minus the true-growth vector yields a vector whose direction (N. 66° E.) matches the direction of the freshest east-flank striations (fig. 10*B*). Deformation patterns east of the spine thus suggest a simple explanation in which the fresh striations recorded a growth direction relative to debris being dragged southward, and the faint striations recorded the true growth direction of the spine.

Continuing Recumbent Growth of Spine 3

Through November, spine 3 continued to advance to the south-southeast (S. 19° E. to S. 23° E.) at a linear rate of 10–11 m/d (fig. 7). Judging from the slope of the northern face, initial vertical components of motion were ~30°. As features on the spine moved to the south, their vertical motions gradually diminished to zero by ~300 m from the vent, and thereafter they began to subside (LaHusen and others, this volume, chap. 16; this study). The southerly (S. 5° W.) motion of features on the spine turned to south-southeast in mid-November (fig. 7). As the spine axis and growth direction converged, its whaleback form began to take on a smooth gouge-covered appearance on the east and west flanks.

Superposition of spine 3 outlines from November to December 2004 upon the 1986 surface suggests that the growing spine encountered opposing slopes of the 1980 crater wall in mid-November (fig. 8). The surface outline of the spine first overlapped the steep north-sloping crater wall at the bed of the glacier sometime between November 4 and 20 (fig. 12*A*). Northeastward acceleration of GPS spider MID9 north of spine 3 and south of the 1980–86 dome beginning November 12 probably corresponded to the time at which spine 3 began to push against the opposing slope of the 1980 crater beneath the glacier (fig. 13).

As spine 3 continued to impinge on steep, opposing subglacial slopes of the crater wall in late November and December, the spine axis began to rotate eastward (table 2, fig. 12*A*) and the spine began to break. Axis orientation changed 8° eastward from November 20 to December 11 (table 2). Between November 20 and 29, fracturing and separation of the first piece of spine 3 was apparent (figs. 2*A*, 2*B*), consistent with northeastward acceleration of GPS station MID9 during November 23–27 ("1st breakup" in fig. 13*A*). By November 29, this small spine fragment had completely separated, and by December 11, the rotating spine had pushed it into a steaming heap along its margin with east Crater Glacier (fig. 2*C*). A second, more substantial fragment separated and decoupled in early December. Northeastward acceleration and deceleration of MID9 suggests that the period of the fracture and decoupling of the resultant spine fragment spanned December 6–12 ("2nd breakup" in fig. 13*A*).

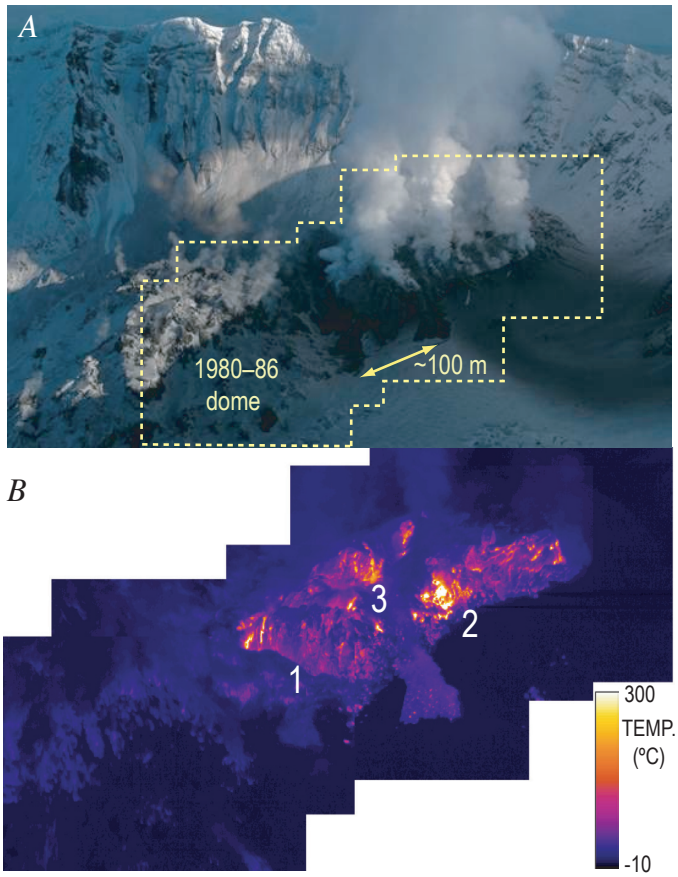

Figure 9. Mount St. Helens crater floor on October 27, 2004; view from northwest, illustrating spines 1–3. *A*, Photograph showing 1980–86 dome and ongoing extrusion, with fresh ash on Crater Glacier west of new dome. *B*, Mosaic of thermal-infrared images located in *A* from same date and time. Numbers indicate spines 1–3. Maximum temperature in field of view is 600°C (scale is set such that all temperatures greater than 300°C are white). Spine 3 has emerged since previous TIR survey on October 24. Thermal imagery shows hot debris fan and hot blocks on ice and firn near spine 1 and between spines 1 and 2. USGS photo by J.W. Vallance; thermal images by D.J. Schneider.

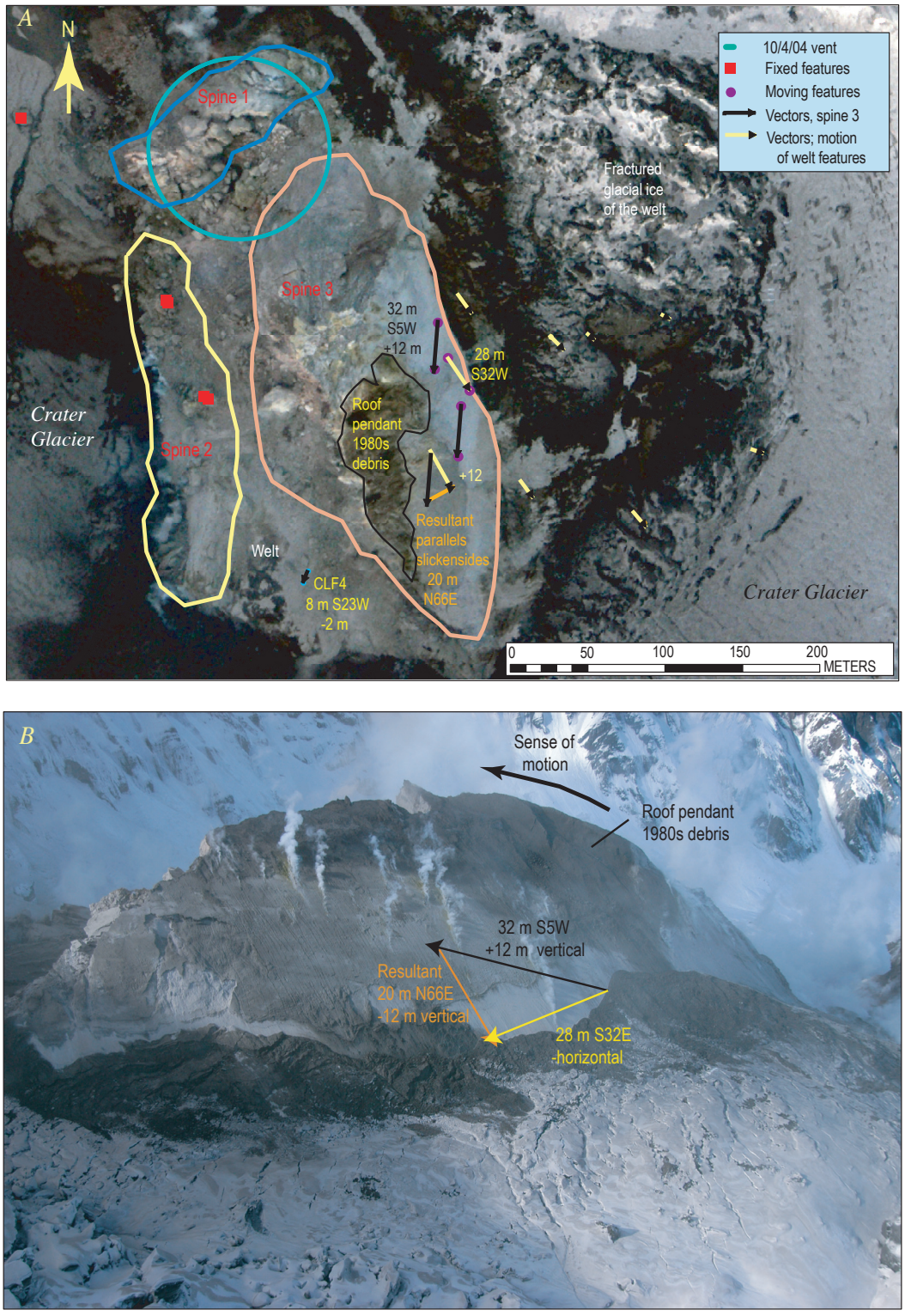

Figure 10. Mount St. Helens crater floor in early November 2004. *A*, Rectified vertical aerial photograph of dome taken November 7, 2004, with handheld camera from an airplane. The photograph was subsequently rectified using features on 1980–86 dome, Opus, and Crater Glacier for both November 4 and 7 so that its central part is tied to geographic coordinates of the November 4 DEM. The aerial photograph shows deformation vectors in plan view for November 4–7. *B*, Oblique photograph looking west at spine 3 on November 4, 2004, showing faint striations parallel to deformation vector, $\vec{V}_{black}$, and young pronounced striations parallel to vector $\vec{V}_{orange}$, where subscripts indicate vector colors in photograph. Debris adjacent to whaleback moves in the near-horizontal plane parallel to $\vec{V}_{yellow}$ such that $\vec{V}_{yellow} - \vec{V}_{black} = \vec{V}_{orange}$. USGS photos by J.S. Pallister.

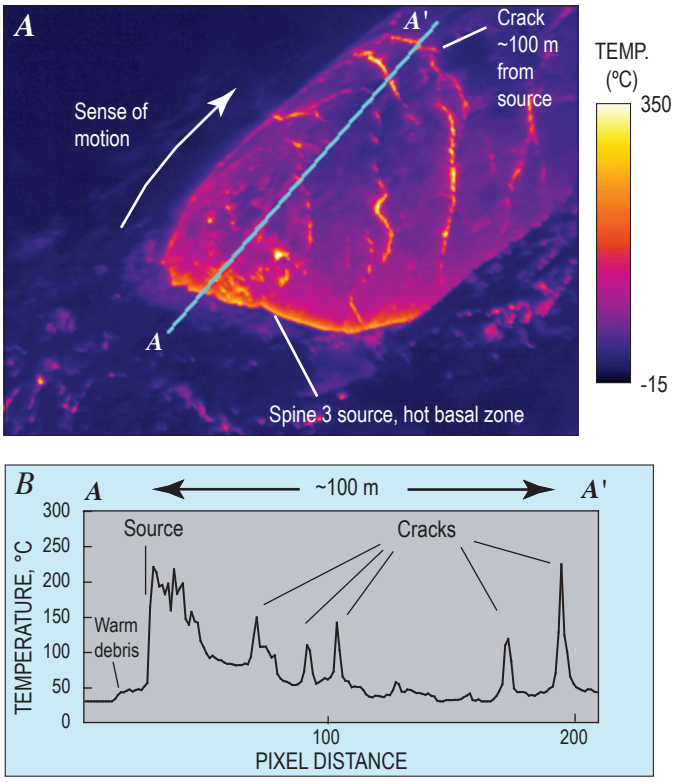

Figure 11. Thermal aspect of spine 3 surface on November 29, 2004. *A*, Thermal-infrared image from helicopter, view to southeast, by J.W. Vallance. *B*, Temperature profile from north to south.

There was no big north-south crack in a December 4 image (R.L. Helz, written commun., 2004). However, a December 8 image revealed a well-developed crack, confirming that during that interval a substantial part of the spine had begun to separate from its west flank along a longitudinal fracture oriented parallel to the spine's axis. December 11 photographs (fig. 2*C*), DEM (Schilling and others, this volume, chap. 8), and geologic map (Herriott and others, this volume, chap. 10) revealed that this fragment had largely decoupled and had begun to subside westward by that date. During November to mid-December numerous other small spine fragments separated from spine 3, mostly to the west. Generally, fragments separating to the west slowly subsided and stagnated, whereas the few separating to the east were bulldozed eastward.

Late October–Mid-December Deformation of Surrounding Areas during Spine 3 Growth

In response to recumbent dome growth from late October to mid-December, areas east of spine 3 rotated eastward about a pivot axis near Opus, showing horizontal displacements as great as 100 m. Areas west of spine 3 subsided or stagnated and moved less than 20 m (figs. 7, 14*A*). All areas east of spine 3 rotated eastward in such a fashion that displacement per unit time increased from north to south. Ice masses on the welt subsided and then migrated eastward across the boundary between stagnant ice and the Crater Glacier, whereupon they began to rise. During this interval all ice on the east Crater Glacier rose between 10 and 50 m, with largest vertical displacements occurring to the south and the smallest to the north (figs. 7, 14*A*). In effect, rotating dome and welt rock bulldozed the glacier eastward, compressing and lifting it such that its cross-sectional profile changed from concave to convex (figs. 2, 14*A*).

Spine 1 moved in response to the emerging spine 3, then stabilized as that new spine continued to grow. Spine 1 was displaced about 40 m north-northwest and tilted from a dip of 50° to 80° northwest between mid-October and early November (fig. 7). Comparison of the October 14 DEM with those of November (figs. 5, 7) shows the change in position of spine 1 with respect to the October 4 vent position. This displacement and rotation coincided with southward growth and emergence of spines 2 and 3. The displacement and rotation were to the northwest, directly away from the origin of spine 3's southward extrusion, and are likely to have been a response to spine 3 emergence rather than growth of spine 2.

Spine 2 and the area between spines 2 and 3 rotated slightly and subsided between October and December. In late October and early November, spine 2 moved as much as 20 m to the northwest at its south end but remained relatively stable to the north. In late October, the top of spine 2 was as much as 20 m higher than the adjacent glacier surface (fig. 9). As spine 3 grew, spine 2 subsided by 20–25 m (fig. 7). By late November, spine 2 had become a nondescript entity hidden below the level of west Crater Glacier, with talus and rockfall encroaching upon it from the more prominent spine 3 to the east (fig. 2*B*). The GPS spider CLF4, placed on the welt October 27, was perched between spines 2 and 3 as spine 3 emerged. The spider had moved ~44 m S. 24° W. and subsided 13 m by November 19, when it was buried by rockfall from spine 3 (LaHusen and others, this volume, chap. 16). As spine 3 advanced, it pushed parts of the dome south and west of it to the southwest, but, after its leading edge passed by and the spine began rotation in the opposite direction, subsidence of areas west of spine 3 began—possibly caused by removal of buttressing from the east.

West Crater Glacier, south and west of the spine complex, responded during a brief interval as spine 3 approached but otherwise remained relatively static from late October to mid-December (fig. 7). Dome growth after November 4 caused no detectable deflection of west Crater Glacier. A slow increase in altitude of the west glacier, caused in part by accumulation of snow, occurred as spine 3 grew. Areas of the glacier immediately south of the dome complex moved tens of meters as the whaleback approached (fig. 7), but then they stopped.

Breakup of Spine 3 and Formation of Spine 4: December 18, 2004–April 8, 2005

Spine 3 broke up and decoupled as spine 4 formed between mid-December 2004 and early January 2005. Photograph sequences showed fractures oriented diagonally across

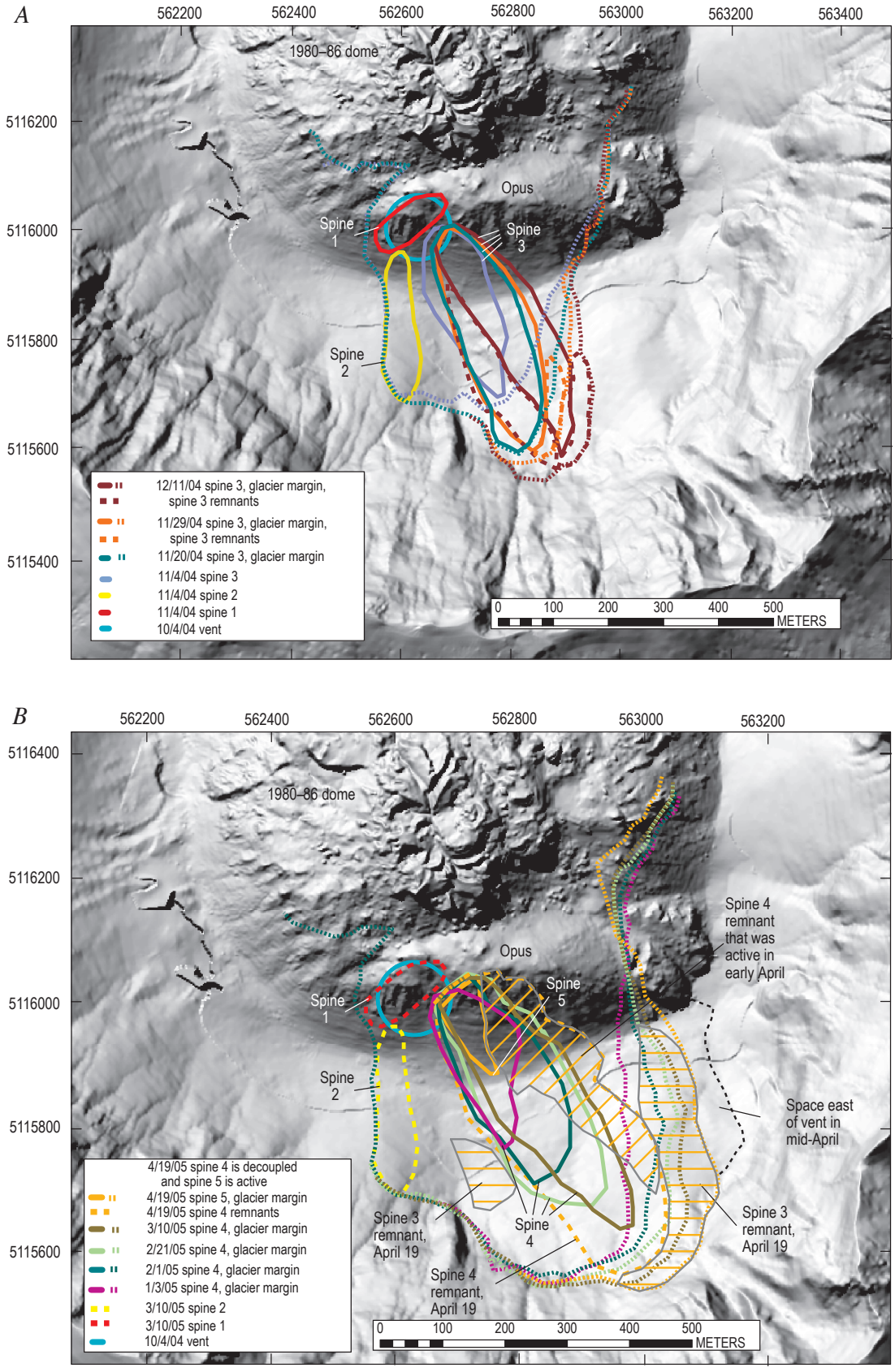

Figure 12. Outlines of active spines and dome-glacier margins at Mount St. Helens, Washington, superimposed on 1986 DEM. *A*, November 4–December 11, 2004. *B*, January 3–April 19, 2005.

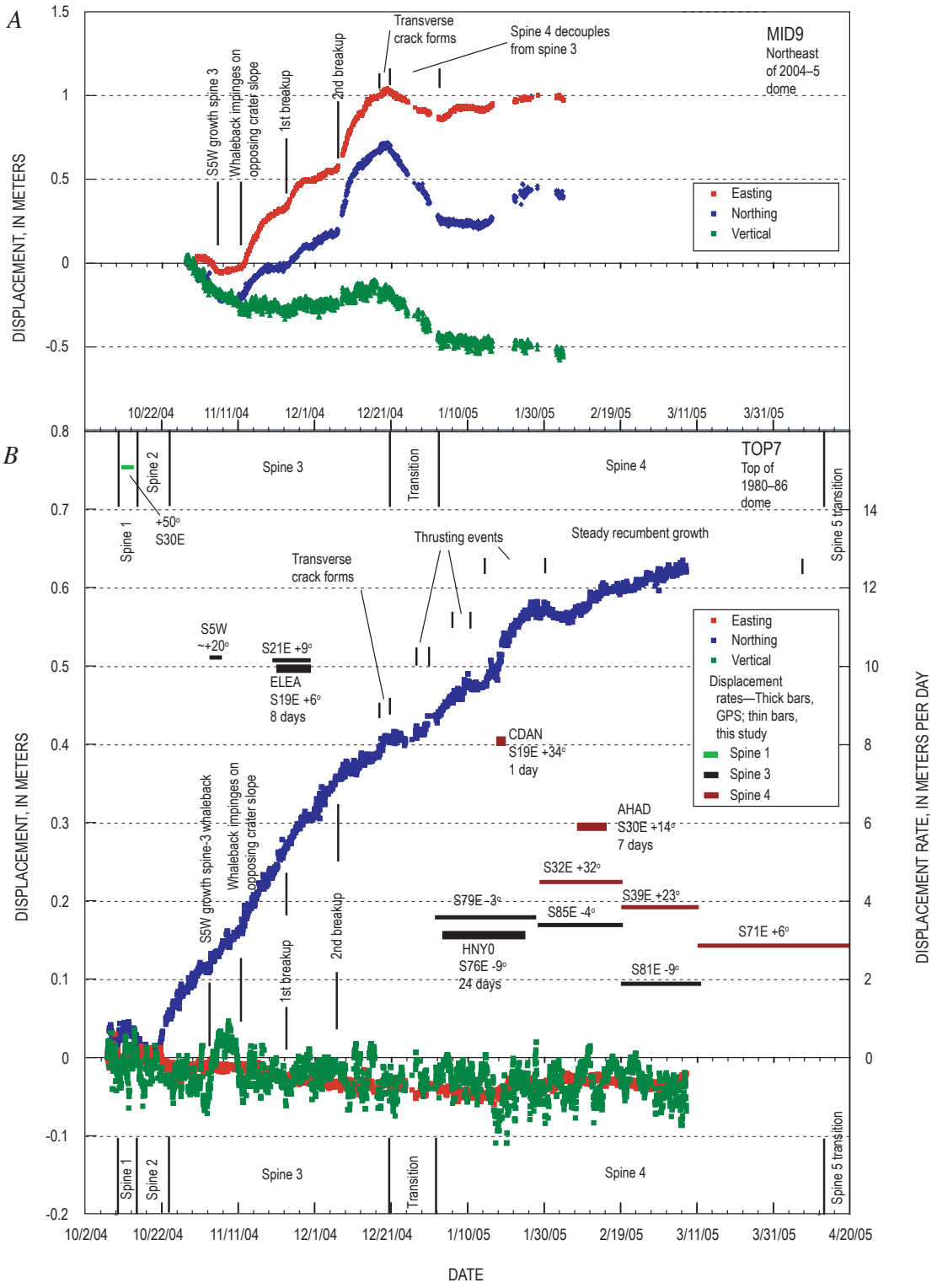

Figure 13. Plots of displacement versus time for GPS stations MID9 (*A*), located between 2004–5 and 1980–86 domes, and TOP7 (*B*), located at apex of 1980–86 dome, with intervals of spine growth and key events during spine growth, as well as linear extrusion rates of GPS receivers and features tracked in this study superimposed on GPS time series. Initial locations shown in figures 7 and 15. Because of their locations just northeast and north of spines 3 and 4, MID9 and TOP7 stations commonly accelerated opposite spine growth when spine met resistance to its growth and decelerated when that resistance was relieved. GPS data from LaHusen and others (this volume, chap. 16).

spine 3 that formed and became more prominent beginning about December 18 (Major and others, this volume, chap. 12). Station MID9 reversed its direction of motion from northeast to southwest on December 20 (LaHusen and others, this volume, chap. 16), an event correlated approximately to the formation of the transverse fractures (fig. 13). Southward thrusting of spine 4 over the slowing bulk of spine 3 had become evident by December 24–28 (figs. 2*D*, 2*E*; supplementary movie 2 in Iverson and others, 2006). A second fracture south of the first formed by January 3, 2005, and the decoupling of spine 4 from spine 3 could be considered complete by that time (fig. 2*E*). We infer that cessation of MID9's southwestward motion on January 3 corresponded to complete decoupling of spines 3 and 4.

Between January 3 and April 2005, spine 4 pushed south-southeast from a source located ~70 m east of spine 1. Spine 4 had whaleback morphology similar to that of spine 3 but underwent several cycles of thrusting over spine 3 before it established steady near-uniform growth. Photographs (figs. 2*E*, 2*F*) and time-lapse video (Iverson and others, 2006; Major and others, this volume, chap. 12, appendix 1) reveal thrusting events during January 6–12 and January 14–February 2. The TOP7 GPS spider accelerated northward during each of these events (fig. 13*B*). Time-lapse photography and GPS records for the period of February 2–April 9, 2005, suggest nearly uniform, steady southward growth and no further thrusting events.

By early January spine 4 had a crest oriented S. 27° E. and dimensions of 210×130 m (table 2, fig. 15). Spine 4 grew to ~440 m in length by early March before beginning to break up in April (fig. 16). As with spine 3 during November and December, the long axis of spine 4 began to pivot eastward about its origin at the vent. This rotation began once the spine started to impinge on slopes of the crater wall (figs. 12, 17); its long-axis orientation swung 12° eastward between mid-February and its breakup in mid-April (table 2, fig. 12*B*). This response suggests that the moving spine extended deep enough to be influenced by the slopes of the 1980 crater at depth, as modeled in cross sections (figs. 16, 17).

Linear extrusion rates of spine 4 diminished during January 3–April 10, as shown by analysis of photographs taken at hourly to daily intervals from fixed sites at the eastern crater mouth (Sugar Bowl) (Major and others, this volume, chap. 12), the motions of GPS spiders on the spine (LaHusen and others, this volume, chap. 16), and time-averaged results from this study (fig. 13, table 2). A GPS station, CDAN, moved 8 m/day along a path of S. 19° E. and 34° upward between January 15 and 16. A second station, AHAD, moved 5.9 m/d along a path of S. 30° E. and 14° upward between February 8 and 15 (fig. 13) (LaHusen and others, this volume, chap. 16). A rate and direction estimate using features on successive DEMs for the longer interval between February 1 and 21 was slower: 4.5 m/d along a path of S. 32° E.

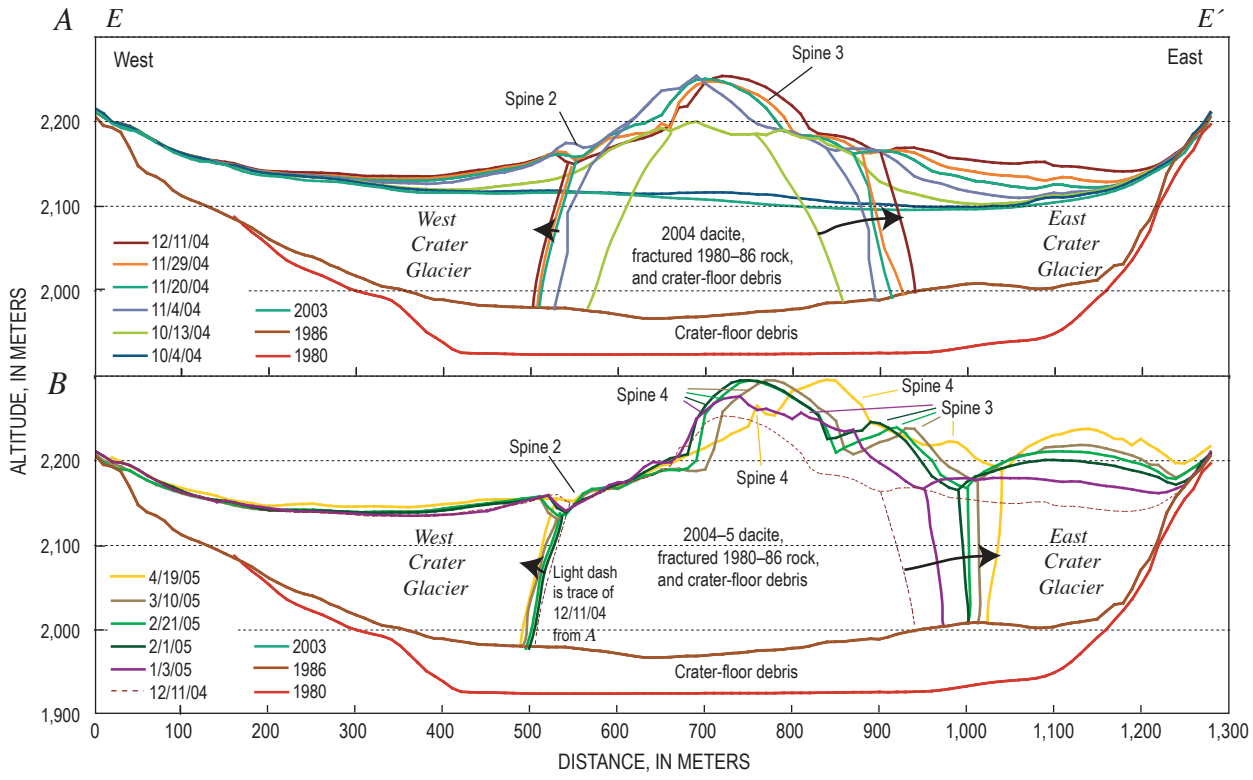

Figure 14. East-west cross section ***E–E´*** (location shown in figures 1 and 7) illustrating response of glacier to recumbent growth of spine 3. *A*, Profiles for October 13–December 11, 2004. *B*, Profiles for January 3–April 19, 2005.

and 32° upward (figs. 13, 15). This slower rate is about the same as spine 4 extrusion rates reported by Iverson and others (2006) and Major and others (this volume, chap. 12), who compared daily Sugar Bowl photographs. With time, extrusion rates diminished and directions became more easterly: 3.9 m/d along a path of S. 39° E. and 23° upward between February 21 and March 10. This decreased to 2.6 m/d along a path of S. 71° E. and 6° upward between March 10 and April 19. We estimated a time-averaged rate of advance for the period of January through mid-March by measuring advance of the leading edge of the whaleback in cross section (fig. 16). Between January 3 and March 10, the advance of ~300 m gave a rate between 4 and 5 m/d. Rates were as high as 8 m/d during some briefer intervals (table 2).

The initial volume of spine 4 on January 3, 2005, as it splintered from spine 3, was 5.5×10^6 m^3, and total volumes of hot rock reported for different times during the spine 4 extrusion (Schilling and others, this volume, chap. 8) allow calculation of spine 4 volumes and time-averaged, volumetric extrusion rates between January and April 2005 (table 2). Time-averaged extrusion rates for these intervals suggest a spurt in growth from February 1 to 21. The growth spurt occurred during the same interval in which spine 4 transitioned from intermittent thrusting to steady recumbent growth.

Deformation of Areas Surrounding Spine 4 Growth during January–April 2005

Spine 4 growth during January through April caused areas to the east to rotate eastward about a pivot near Opus. Displacements were as great as 200 m (fig. 15). In response to motion of the welt to the south of Opus, ice masses stranded

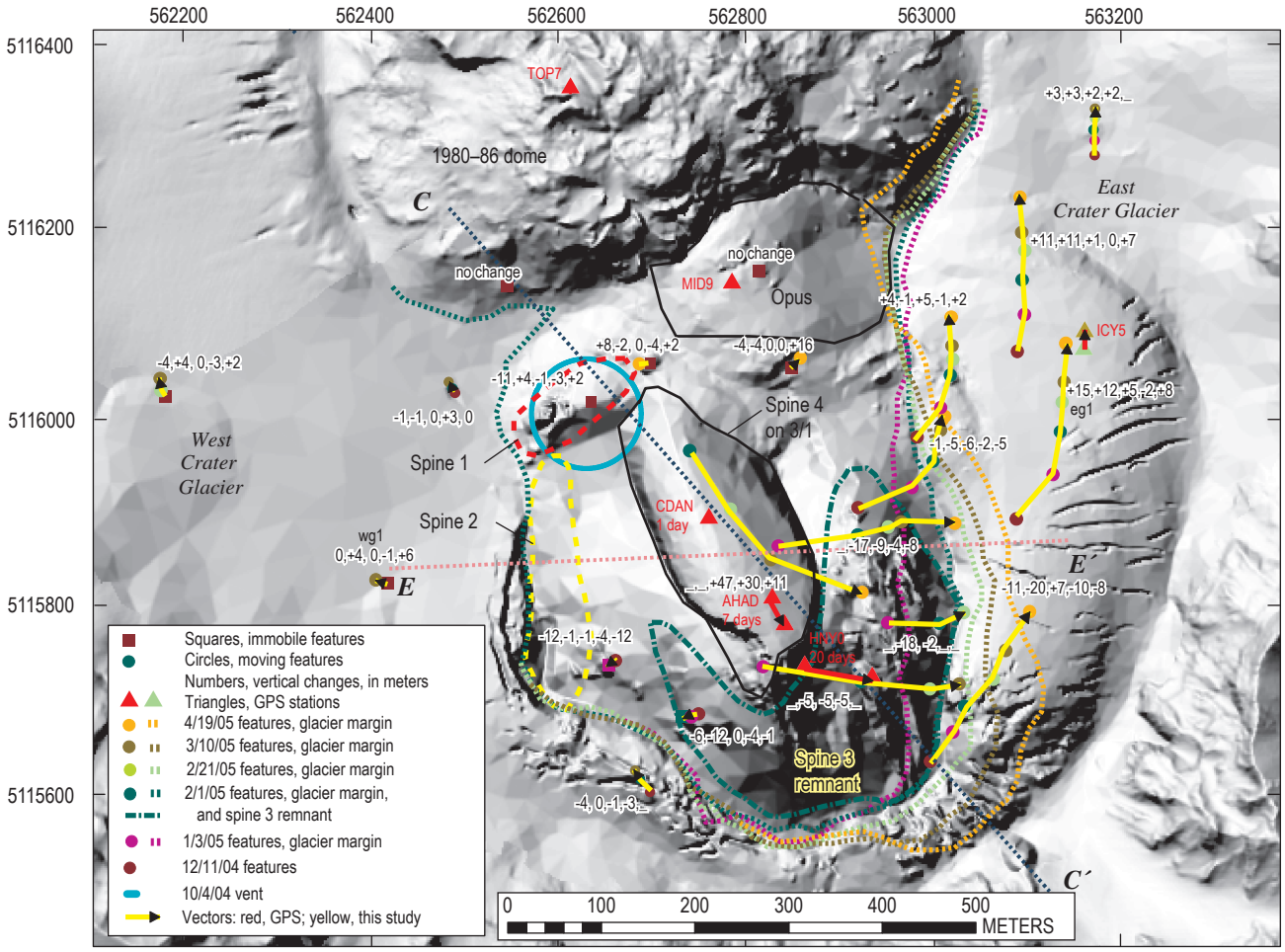

Figure 15. Deformation vectors for the period from January 3 to April 19, 2005, shown on DEM of February 1, 2005. Squares and dots indicate features tracked for dates identified by color in key. These colored symbols delimit deformation vectors of each of the five time intervals between relocation of features. Numbers are vertical components of vectors, in meters, for each interval. Underscores indicate no data for that interval. Dotted lines indicate dome-glacier margins for dates indicated by color in key. Dashed lines ***C–C´***, and ***E–E´*** are traces of cross sections shown in figures 16 and 17.

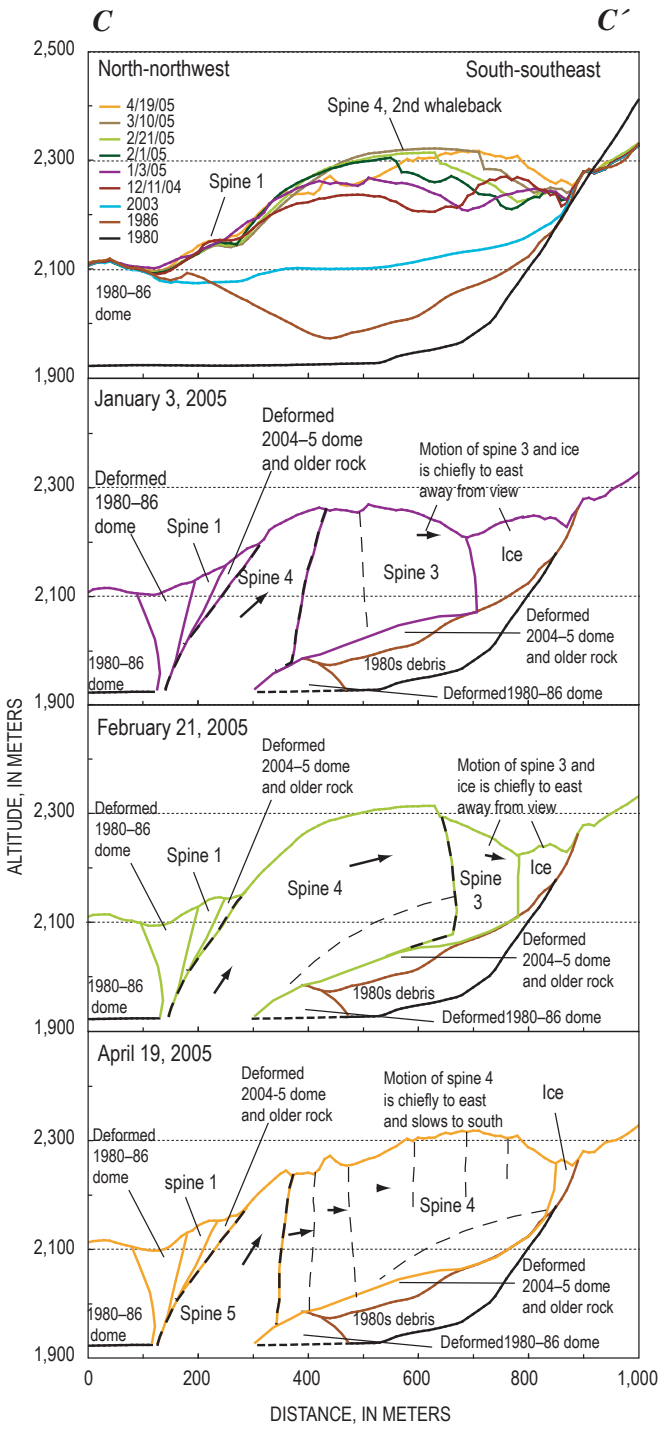

Figure 16. North-northwest to south-southeast cross section *C*–*C´* (location shown in figure 15) illustrating extrusion and recumbent growth of whaleback, spine 4. Top panel shows known profiles for dates given, and other panels illustrate geologic interpretations on given dates. Dashed lines indicate inferred faults.

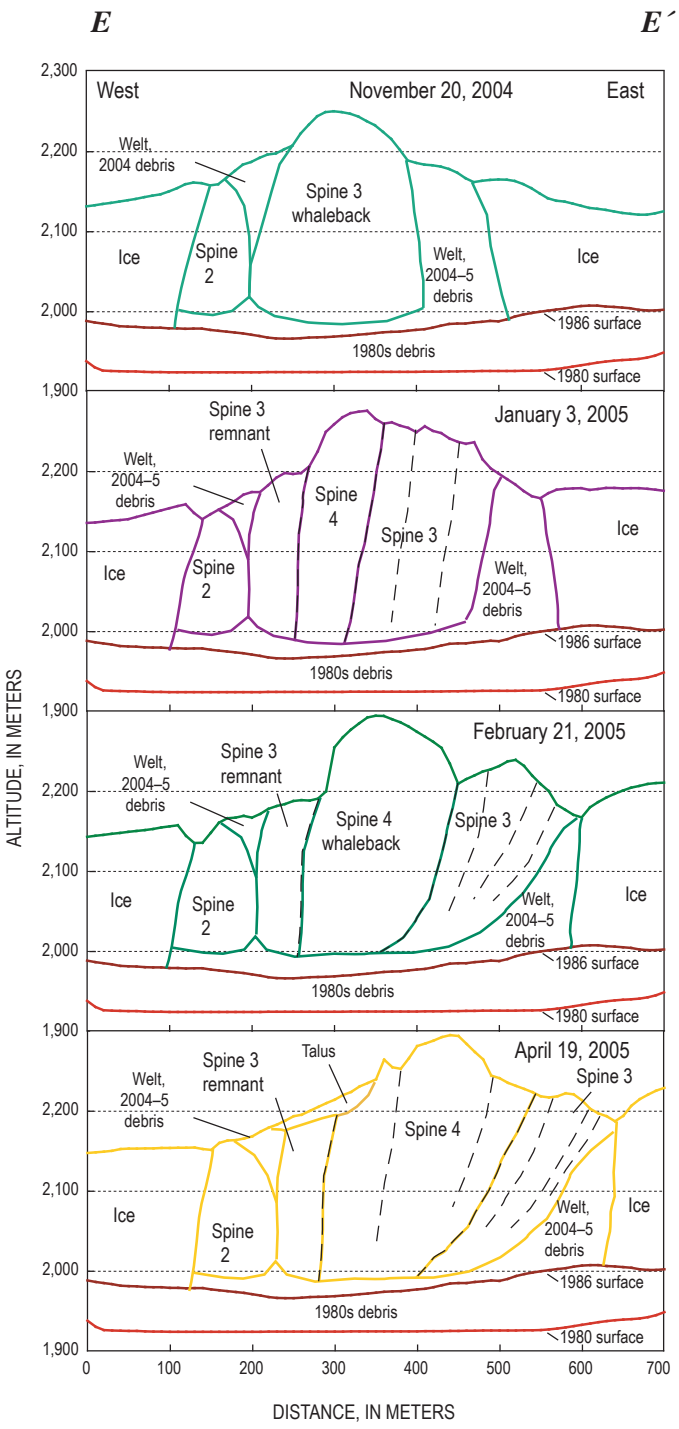

Figure 17. East-west cross section *E*–*E´* (location shown in figure 15) illustrating extrusion and recumbent growth of spines 3 and 4. Panels illustrate geologic interpretations on given dates. Dashed lines indicate inferred faults; heavy and light line weights indicate contacts between spines and within spines, respectively.

on the welt moved eastward until they crossed into the realm of the active east Crater Glacier, whereupon they flowed northward as part of the glacier. Recognizable remnants of the disintegrating spine 3 shifted eastward 100 m or more by February 1. Areas closest to spine 4 moved fastest. Between January 3 and February 1, an area on spine 3 south of spine 4 moved 107 m S. 79° E. at a rate of 3.7 m/d and subsided slightly (fig. 15). The GPS station HNY0, located ~40 m to the east, moved 3.2 m/d, S. 76° E., and also subsided (fig. 13) (LaHusen and others, this volume, chap. 16). Continuing deformation at nearby sites was S. 85° E., 3.6 m/d, and S. 81° E., 1.9 m/d, during February 1–March 10 (fig. 15).

Spine 4 bulldozed and tilted spine 3 eastward, rapidly fracturing it and causing it to disintegrate (figs. 2, 3, 17). By April 19, spine 3 had been reduced to a rubbly ridge adjacent to the east Crater Glacier, and its surface area had been reduced by a factor of five (Herriott and others, this volume, chap. 10). Overthrusting caused by eastward rotation of spine 4 as it deflected off the crater wall caused the reduction in area of spine 3 (fig. 17). Except for one small area, spine 3 remnants to the west were buried by spine 4 talus.

Areas on the 2004–5 dome west of spine 4 continued to subside but moved laterally no more than about 10 m. Spine 1 subsided in December but showed no significant motion thereafter. An area near the south end of spine 2 and another on a remnant of spine 3 west of spine 4 moved less than 10 m southwest between January and February and subsided 10–20 m. Thereafter, subsidence continued at a slower pace, and no further translation of these spine 2 and 3 fragments was detectable.

As the east Crater Glacier continued to be bulldozed eastward at rates as high as 1.5 m/d, it rose tens of meters and accelerated downstream. Between mid-December 2004 and mid-April 2005, the glacier profile bulged as much as 90 m and became markedly convex (fig. 14*B*). During this interval, individual surface features on east Crater Glacier rose as much as 50 m, with the largest vertical displacements in areas east and southeast of Opus. In contrast, farther upslope to the south, features lost tens of meters in altitude as they flowed north (fig. 15). Features with eastward components of displacement in the autumn of 2004 shifted to due north displacement during winter 2005 as the glacier accelerated away from the area of constriction between the rotating dome complex and the east crater wall. The glacier had thickened so much since the onset of the eruption (as much as 130 m) that its slope had increased dramatically, and it responded by flowing north to correct the imbalance.

The Crater Glacier west and north of the spine complex responded by moving a few meters northwest during late December to April, in places rising by a few meters. Although dome growth may have had a minor effect on west Crater Glacier (fig. 15) during the winter months of 2005, accumulation of snow and normal glacier flow downslope probably accounted for most of the observed change. Areas of the glacier immediately southwest of the 2004–5 dome complex moved about 30 m northwest in response to the approach of spine 4 (figs. 12, 15).

Phase 4, Extrusion of Spine 5 across Previous Spine Debris: April 10–July 31, 2005

Spine 4 broke up, decoupled, and changed direction in mid-April 2005. Continual pressure caused by spine 4 pushing against the opposing crater wall disrupted its steady southward propagation and caused it to break apart. Repeat photographs (Major and others, this volume, chap. 12) and time-lapse photography (Iverson and others, 2006) showed development of northeast- to southwest-striking fractures cutting spine 4 at this time. These fractures became progressively more prominent from April 10 to 19. Between April 19 and 24, as the fractures grew, spine 5 began to thrust over the top of spine 4 remnants. Like spine 4, the spine 5 source was ~50 m southeast of spine 1 (fig. 15).

Spine 5 had decoupled from spine 4 by April 19, though it continued to drag the southern parts of spine 4 southward until mid-May and to displace it to the east through June. Spine 5 displayed a smooth, gouge-covered surface near the vent. It became progressively steeper with time, the slope increasing from 40° on April 19 to 54° on July 14 (fig. 18). The spine tended to fracture and crumble as it grew higher, leading to a substantial breakup and decoupling of the southern section of the spine between mid-June and mid-July. During this interval spine growth began to resemble that of the Mont Pelée spine of 1903, with a steeply thrusting lithic core surrounded by an apron of debris at the angle of repose (Blake, 1990). The thrusting spine 5 acted as the driving force for a conveyer that transported at least half of the volume of the crumbling spine southward to form a ridge of disaggregated rock with a trend of S. 10° E. in mid-June and S. 5° E. in mid-July.

From April to August 2005, we were unable to use surface deformation vectors to make independent measurements of spine growth rate because of plumes that obscured key parts of the spine in aerial photos on two of four dates. A limiting, average, lineal growth rate of 4.3 m/d can be calculated from knowing that spine 5 was 100 m long on April 19 and 340 m long on June 15. Data from Major and others (this volume, chap. 12) suggest that extrusion rates of the smooth northern surface diminished from ~4 m/d in late June to ~2 m/d by early July. Time-averaged volume flux decreased slowly between April and July (table 2).

Deformation of Areas Surrounding Spine 5 from April to July 2005

Deformation of areas surrounding spine 5 showed that the spine was deep seated only near its source and was thrusting upward over previous parts of the dome complex to the south (fig. 19). Spine 4 remnants east of spine 5 rotated northeast or east, with the pivot point about 300 m southeast of the vent in an area of stagnant spine 4 rock (near point -7,-2,-3 in fig. 19). The areas of maximum displacement were in the north adjacent to the vent. Maximum displacement east of the vent on

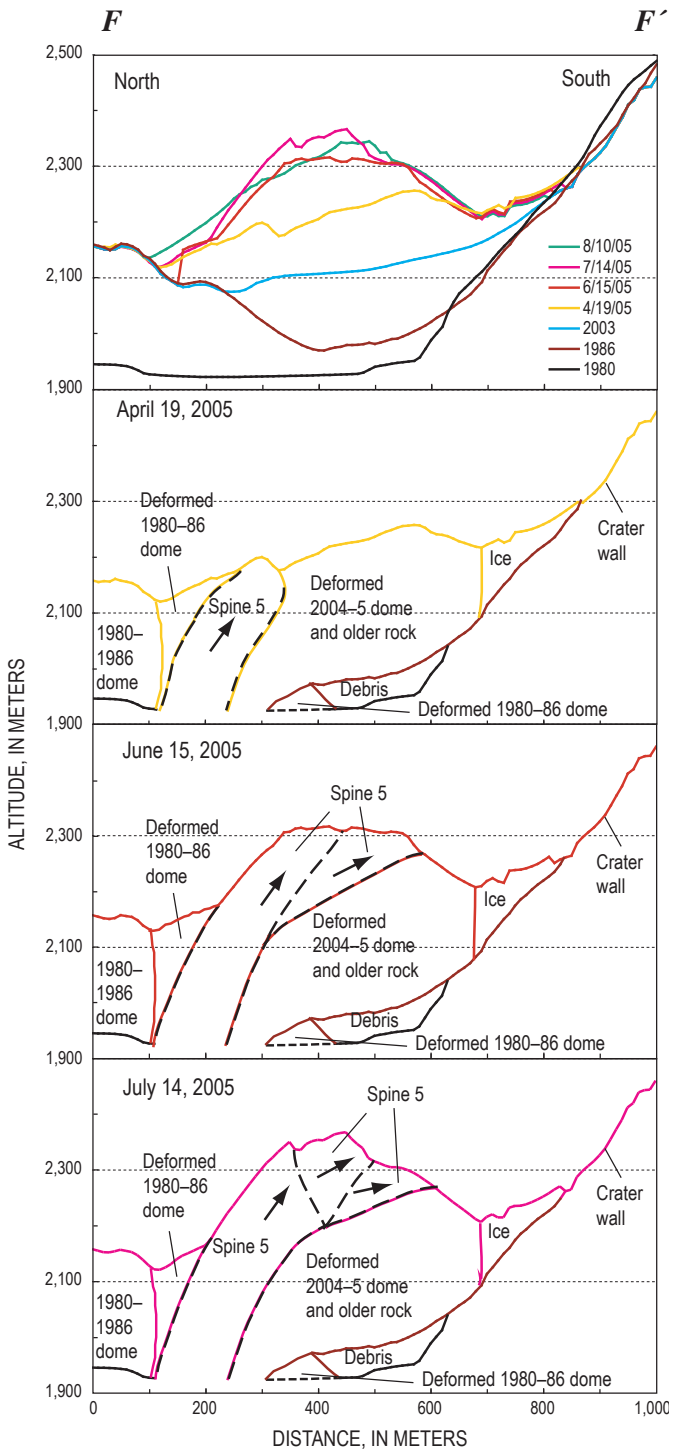

Figure 18. North-south cross section *F–F´* (location shown in figure 19) illustrating extrusion and thrusting growth of spine 5. Top panel shows known profiles for dates given, and other panels illustrate geologic interpretations on given dates. Southern part of spine 5 crumbled and broke up between June 15 and July 14, 2005.

spine 4 was 40–50 m, generally to the northeast. Most of the displacement occurred in April and May; very little occurred thereafter. A feature near GPS station SEV7 moved about 40 m to the northeast and subsided 16 m (point -7, -3, -6, fig. 19). All but 2 m of translation had occurred by June 15, but subsidence continued through August. The GPS station SEV7, located ~30 m west of this feature, was deployed on May 24. By June 15 it had moved only 7 m S. 70° E., implying that about 80 percent of the translation in this area had occurred between the time of the April 19 DEM and May 24. All remnants of spine 4, including those that did not translate significantly, subsided 10–20 m during spring and early summer of 2005. Farther east, spine 3 remnants also subsided between April and June but did not translate more than ~5 m.

Areas on the dome west and north of spine 5 moved northwestward 40–60 m (fig. 19). Spine 1 was pushed ~50 m northwest (point +10, fig. 19). An isolated remnant of spine 3 to the southwest of spine 5 (point -1, fig. 19) moved about 40 m westward before it was buried. Spine 2 was buried by encroaching spine 5 talus in June and then could not be tracked, but its contact with the west Crater Glacier receded as much as 100 m westward between April 19 and August 10 (fig. 19).

Nearby parts of the west Crater Glacier began to be pushed westward and were uplifted (fig. 19). Traceable features on the west glacier moved west as much as 80 m and rose as much as 20 m near the new dome's southwest margin, but areas farther to the north and west merely flowed downslope. Station WES6, a GPS receiver located on the west glacier ~200 m west of the dome, moved 10 m N. 51° W. and rose 0.8 m between July 14 and August 10. Meanwhile, the east Crater Glacier flowed passively to the north. East Crater Glacier fractured and became greatly crevassed as it descended rapidly to the north in response to the 100 m of excess thickness it had gained between November 2004 and April 2005. No further deformation of the east glacier occurred after mid-May, and its boundary with the dome became fairly stable (fig. 19).

Phase 5, Spines 6 and 7 Extrude Westward: August 1, 2005–April 2006 (Ongoing)

Normal Faulting and Westward Growth of Spine 6: August 1–October 9, 2005

Crumbling of spine 5 presaged reorganization of the vent and growth of spine 6 in late July and early August 2005. At least seven substantial rock avalanches and two slumping events between July 18 and 31 (table 3) reduced the smooth steep (54°) slabs of spine 5 of July 14 (fig. 3) to a rubbly ridge by August 10 (fig. 3). During this period, southward motion of segments of spine 5 slowed successively from south to north in such a way that, by the end of July, only the northernmost segment remained active.

During a transitional period August 1–5 (table 1), spine motion seen in time-lapse photography (Iverson and others, 2006) became localized to the vent area, where the sense of

motion was nearly vertical, as the remainder of spine 5 began to slump slowly. A fracture system, somewhat concealed by rubble, developed along a S. 10° W. trend and divided the stagnating spine from the active extrusion as spine 6 developed and became the dominant feature, evident in images of August 10, 2005 (fig. 3).

From early to mid-August, spine 6 began moving westward, slowly at first but then more rapidly. This westward motion of the extruding mass beginning on about August 6 marked the completion of the transition from spine 5 to spine 6 (table 1). Time-lapse photography of August 6–12 (Iverson and others, 2006) showed that spine 6 disintegrated continuously as it extended to the west.

The spine 6 mass comprised buried spines 1 and 2, a substantial part of spine 5 that had slumped to the west, debris shed from spines 3, 4, and 5, and welt rock caught between spines 1, 2, and 3 (fig. 20). This mass thus included massive lava, as well as deformed and disintegrating blocks and debris. On August 10, the extruded lava volume in spine 6 was ~1×10^6 m^3, but the total volume of the deformed mass was ~12×10^6 m^3 (table 2). A spurt in lava extrusion occurred during the transition from spine 5 to spine 6 and continued into September (table 2).

No specific feature on spine 6 could be tracked in DEMs and vertical aerial photos between August 10 and September 20. However, the trace of the active spine and the shift of the west glacier-spine margin constrain the magnitude of translation during this period (fig. 21). The most active part of the spine migrated ~140 m N. 75° W. during the 41 days at an average rate of 3.4 m/d. Overall the most active part of the spine subsided a net ~40 m, but this value ignores vertical growth—active disintegration removed tens of meters from the apex of spine 6. The center of most active extrusion moved westward away from the original (October 4, 2004) vent area

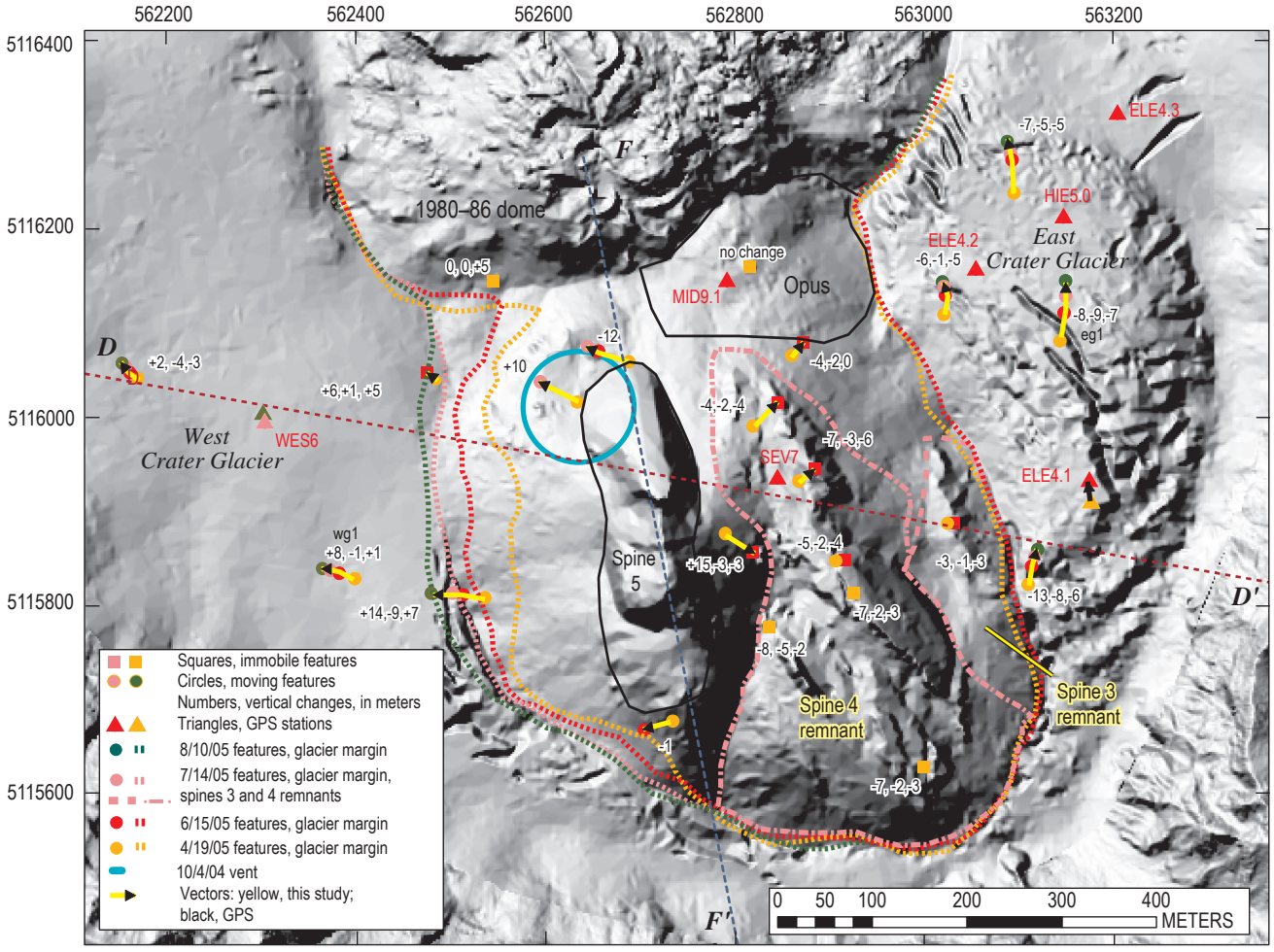

Figure 19. Deformation vectors for the period from April 19 to August 10, 2005, shown on DEM of July 14, 2005. Squares and dots indicate features tracked for dates identified by color in key. These colored symbols delimit deformation vectors of each of the three time intervals between relocation of features. Numbers are vertical components of vectors, in meters, for each interval. Underscores indicate no data for that interval. Dotted lines indicate dome-glacier margins for dates indicated by color in key. Line ***F–F´*** is trace of cross section shown in figure 18; line ***D–D´*** is trace of cross section shown in part in figure 22.

Table 3. Timing, style, and direction of mass-wasting events from spine 5 at Mount St. Helens, Washington, July 19–31, 2005.

[Timing and style of phenomena are inferred from time-lapse video (Iverson and others, 2006).]

Interval during which event occurred	Phenomenon	Direction
July 18–19	Avalanche	East
July 19–20	Avalanche	West
July 20–21	Avalanche	West from near apex of smooth slab
July 22–23	Avalanche	West
July 23–25	Slump	West
July 26–27	Avalanche	East
July 27–29	Slump	West from rubbly area of south part of spine
July 28–29	Avalanche	East
July 30–31	Avalanche	West

(fig. 21). Along an arc west to southwest of this new vent, the glacier-spine 6 contact receded 60–90 m westward at an average rate of 1.5–2.2 m/d (figs. 20–22).

Spine 5 Subsidence and Deformation of Surrounding Areas during August–September 2005

All parts of spine 5 translated westward and subsided as spine 6 moved away and removed its westward buttress (figs. 21, 22). Areas near spine 6 experienced maximum displacements of 40–60 m to the west and subsided by as much as 65 m. Areas close to the crest of spine 5 dropped by as much as 50 m while translating ~20 m westward. Such a pattern implies normal faulting along a northerly strike with westward dip as steep as 70°. The principal fault surface appears to coincide with a subsurface boundary sloping steeply to the west and demarcated by the contact between the subsurface remnants of spines 4 and 5 (fig. 22). This boundary could have formed a weak surface that was susceptible to subsequent subsidence. Features on spine 5 farther west of the fault trace translated more and subsided less than those near it, a pattern that implies rotational motion along a flattening fault (fig. 21). We infer that the fault is listric, dipping steeply westward along its near-surface trace and flattening as it extends deeper to the west (fig. 22).

The perspective provided by south-rim time-lapse photography (Poland and others, this volume, chap. 11) suggests that southwestern parts of spine 5 and southeastern parts of spine 6 subsided and migrated westward in tandem. Spine 5, near its eastern margin, subsided very little, apparently because the underlying spine 4–5 contact dipped gently compared to the steeper contact to the west. The most significant translation had occurred by September 20, but some areas continued to subside through October. Subsidence of spine 5, coupled with westward extension of spine 6, resulted in formation of a sag between spines 5 and 6 (figs. 21, 22).

To the east, Opus, spine 3, and spine 4 were relatively immobile, moving less than 4 m. In August and September, the GPS station SEV7, situated on spine 4 about 30 m to the east of spine 5, translated 2 m westward and subsided 3 m as the spine 5 buttress gave way. Motion on other parts of Opus, spine 3, and spine 4 was too small to be detectable (fig. 21).

While west Crater Glacier accelerated westward to northwestward and thickened, east Crater Glacier continued to flow passively northward (fig. 21). Between August 10 and October 24, traceable features on the west glacier moved west by 100–120 m and rose 20–35 m in response to the bulldozing caused by spine 6 advance (fig. 22). Ensuing crevasses radiated westward along the principal strain axis. Three GPS stations were located on west Crater Glacier for various time intervals (Walder and others, this volume, chap. 13). An example, WES6, originally about 150 m west of the dome, moved 50 m N. 51 W. and rose 13 m during August 10–September 14. In contrast, its motion in the 27 days before August 10 was only 10 m northwest and 1 m up. Advance of spine 6 pushed west Crater Glacier westward and heaped it as high as 30 m above its previous surface.

Westward Extrusion and Overthrusting of Spine 7: October 9, 2005–April 2006

Extrusion of spine 7 began in mid-October with subsurface spine intrusion centered east of spine 6 and near the trace of the October 4, 2004, vent. Subsurface intrusion gave way by November to spine extrusion, which continued through April 2006 (table 1, fig. 21*B*).

An increase in high-frequency earthquakes, beginning on October 9, 2005, marked the beginning of spine 7 growth (Moran and others, this volume, chap. 2). Fuming and heating of the surface area above the October 2004 vent observed in thermal images of October 11, 2005, revealed the first surface manifestation of the new intrusion (fig. 3). Time-lapse photographs from a camera on the south crater rim (Poland and others, this volume, chap. 11) showed general bulging of a rubbly area between spines 5 and 6 by October 13.

Uplift and westward motion that became increasingly evident between October 14 and 21 indicated extrusion of spine 7. From its origin in the depression between spines 5 and 6, spine 7 pushed upward and outward to the west, steepening on the east as it grew and overthrusting spine 6 to the west (fig. 20). By mid-November, a broken-up slabby spine had begun to emerge from the rubble-strewn slopes of the bulge. By mid-December, this slab of rock had become more coherent and prominent. As it continued to grow, the slab steepened eastward progressively, attaining a slope of 50° by April 2006. The extruding slab also pushed spine 6 and part of spine 7 across a sector extending from southwest

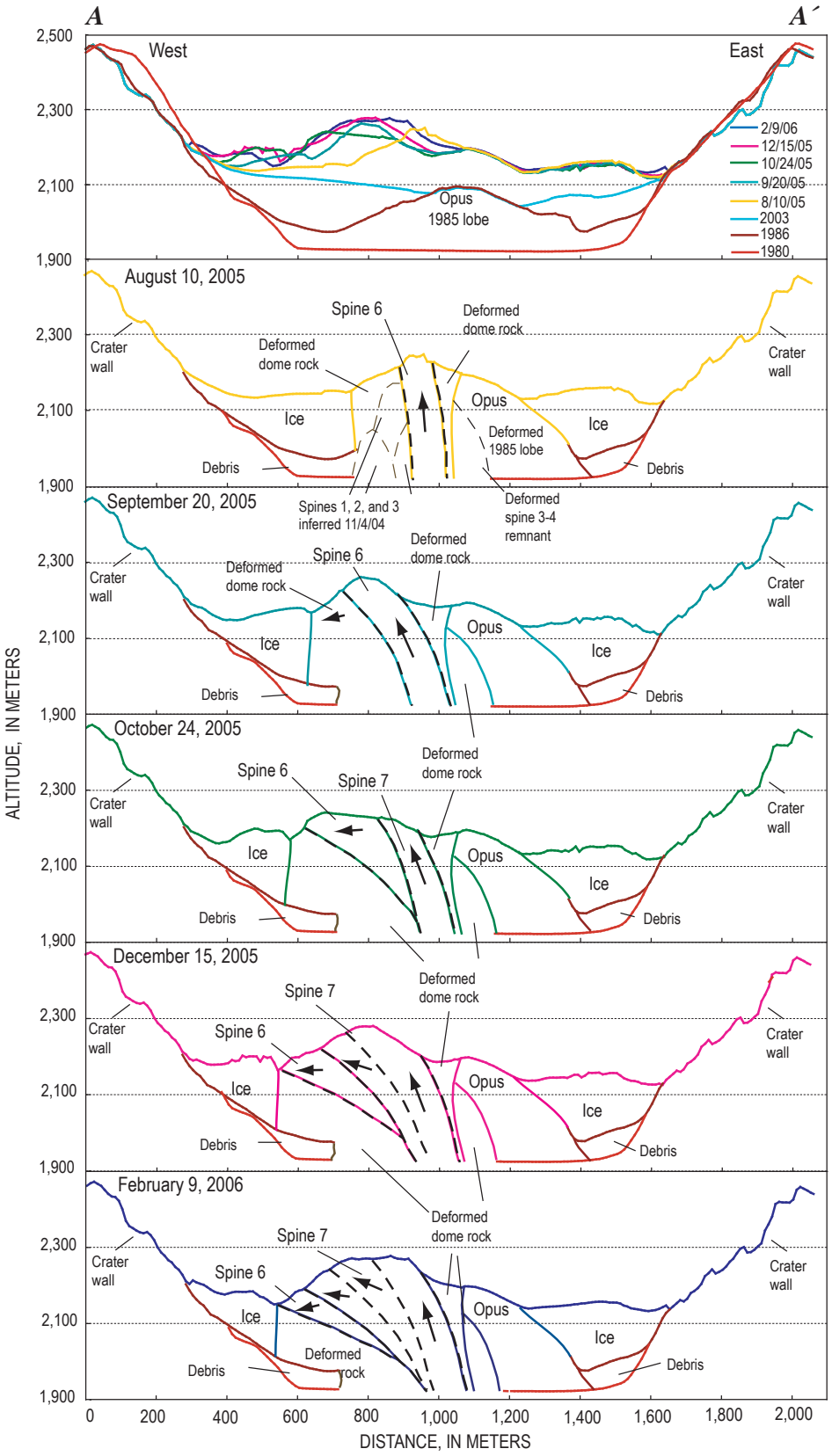

Figure 20. East-west cross section *A*–*A´* (location shown in figures 1 and 21) illustrating extrusion and thrusting of spines 6 and 7. Top panel shows known profiles for dates given, and the other panels illustrate geologic interpretations at labeled times. Dashed lines indicate thrust faults.

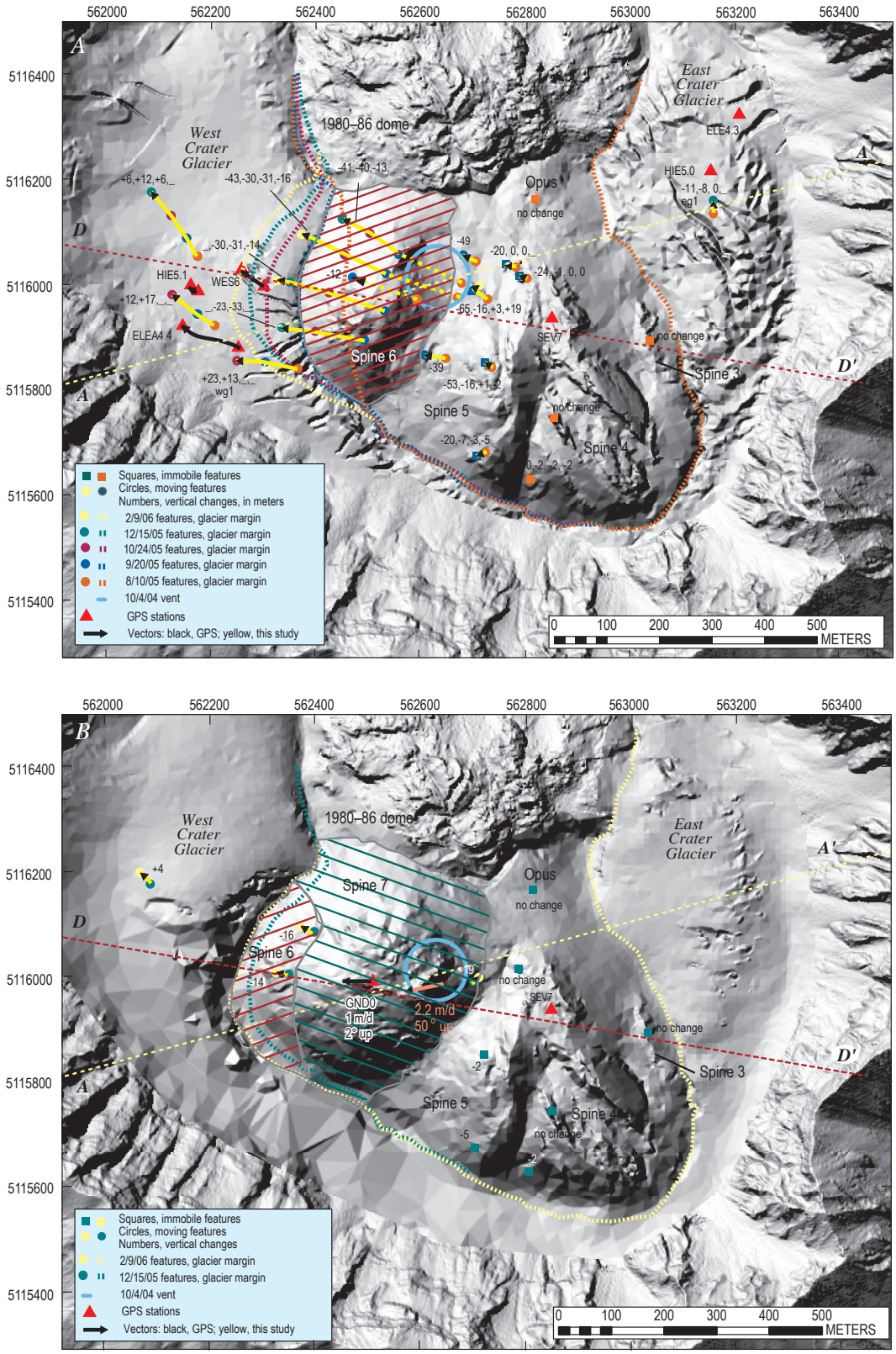

Figure 21. Deformation vectors for the period from August 10, 2005, to February 9, 2006, shown on DEMs. Squares and dots indicate features tracked for dates identified by color in key. These colored symbols delimit deformation vectors of each of the time intervals between relocation of features. Numbers are vertical components of vectors, in meters, for each interval; underscores indicate no data for interval. Red-lined pattern indicates spine 6; green-lined pattern indicates spine 7. Dotted lines indicate dome-glacier margins for dates indicated by color in key. Lines ***A–A´*** and ***D–D´*** are traces of cross sections shown in figures 20 and 22. *A*, September 20, 2005. *B*, February 9, 2006.

to northwest radially away from its source (fig. 21). Rock debris continually avalanching from the west face of spine 7 formed hot talus slopes on this side. As the spine grew through November, its rubbly western slope began to bury adjacent sections of spine 6.

Spine 7 formed a distinct entity between, and overlapping, spines 5 and spine 6. By October 24, the spine had been extruding for 10 days, and we estimate its volume as about a third of the total volume erupted since September 20, or ~1×10^6 m^3. Between October 24, 2005, and February 9, 2006, time-averaged magma flux gradually diminished (table 2).

As spine 7 moved westward and thrust over spine 6, it grew higher and steeper, and its solid eastern buttress became a progressively more prominent, finlike structure (figs. 23*A*, 23*B*). Cracks penetrated the gouge coat in distinctive patterns and moved upward and westward along with the fin (fig. 23*A*). From examination of photographs, spine 7 was ascending westward at an angle of 50° at a rate of ~2 m/d in early April (fig. 23*A*). At the same time, GPS station GND0, ~100 m west of the fin, was only moving 1 m/d horizontally westward (fig. 23*C*). This discrepancy in rate of deformation within spine 7, with steeper, faster displacement near source and slower subhorizontal displacement to the west, implies internal shearing (figs. 20, 23*D*).

Deformation during Spine 7 Extrusion: October 9, 2005–April 2006

All parts of spine 6 translated and subsided as spine 7 pushed it westward (figs. 21, 22). Features on spine 6 were subject to substantial but gradually diminishing deformation from October 9, 2005, to February 9, 2006, with maximum total displacement over this period in excess of 200 m to the west and subsidence as much as 80 m (table 4). Toward the end of this period, spine 7 moved about 1 m/d westward with no subsidence, while adjacent spine 6 moved at half that rate and subsided (table 4). Such a pattern implies shearing between spines 6 and 7 (figs. 20, 23*D*).

West Crater Glacier continued to move westward to northwestward (fig. 21). Between October and December, a single traceable feature on the west glacier moved northwest 60 m and rose 6 m in response to continuing spine impingement (fig. 21). Motion of GPS station ELE4.4, positioned farther south and closer to spine 7, slowed after October 24. It moved 1.6 m/d N. 68° W. and rose 19 m in the 34 days before October 24, whereas it moved 1.1 m/d N. 55° W. and rose 3 m in the 15 days after that date (LaHusen and others, this volume, chap. 16). Farther north, the glacier accelerated to the north in response

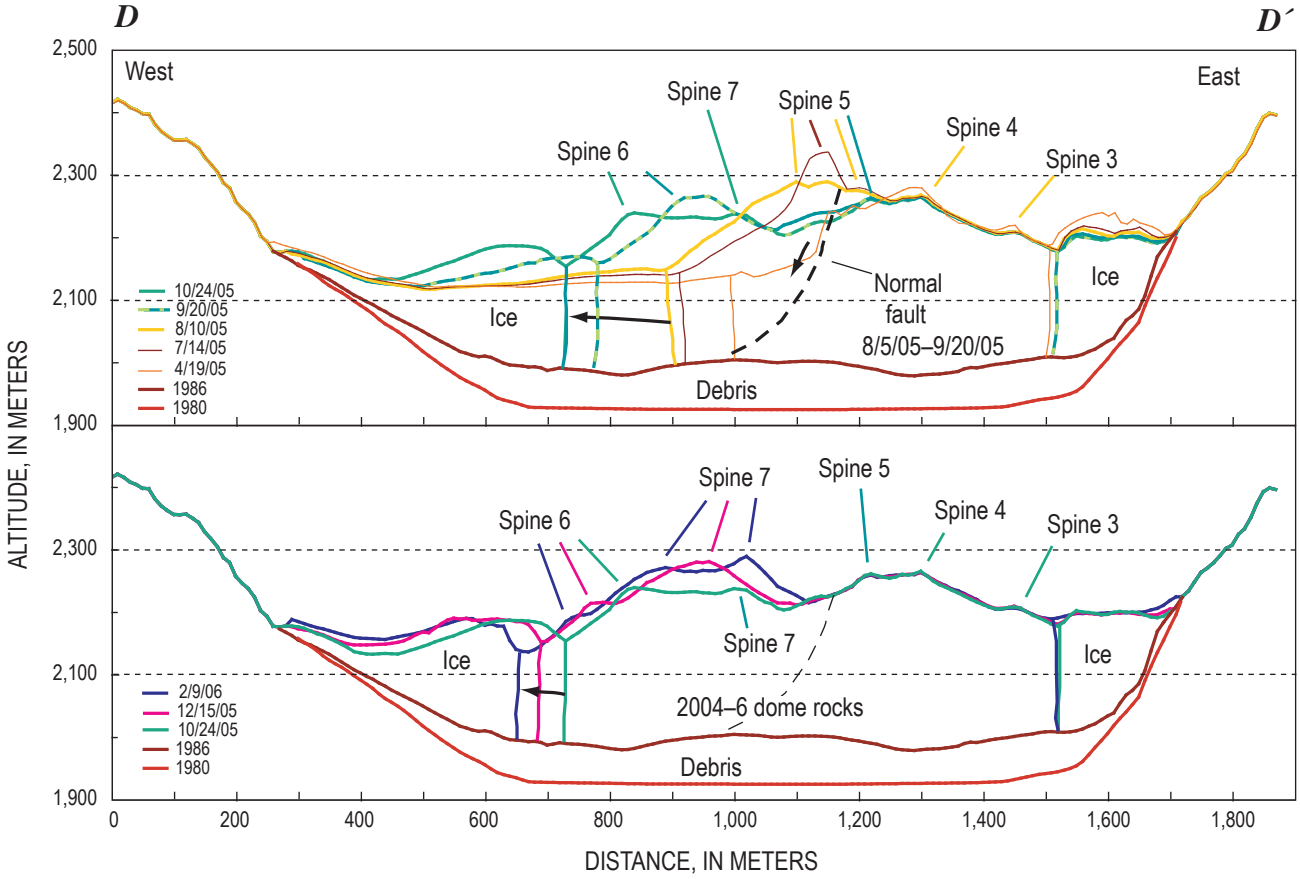

Figure 22. East-west cross section *D*–*D´* (location shown in figures 1 and 21) illustrating extrusion and thrusting of spines 6 and 7. Panels illustrate geologic interpretations at labeled times. Dashed line indicates inferred normal fault, which is located at steep west-dipping trace of spine 4 on April 19, 2005, surface.

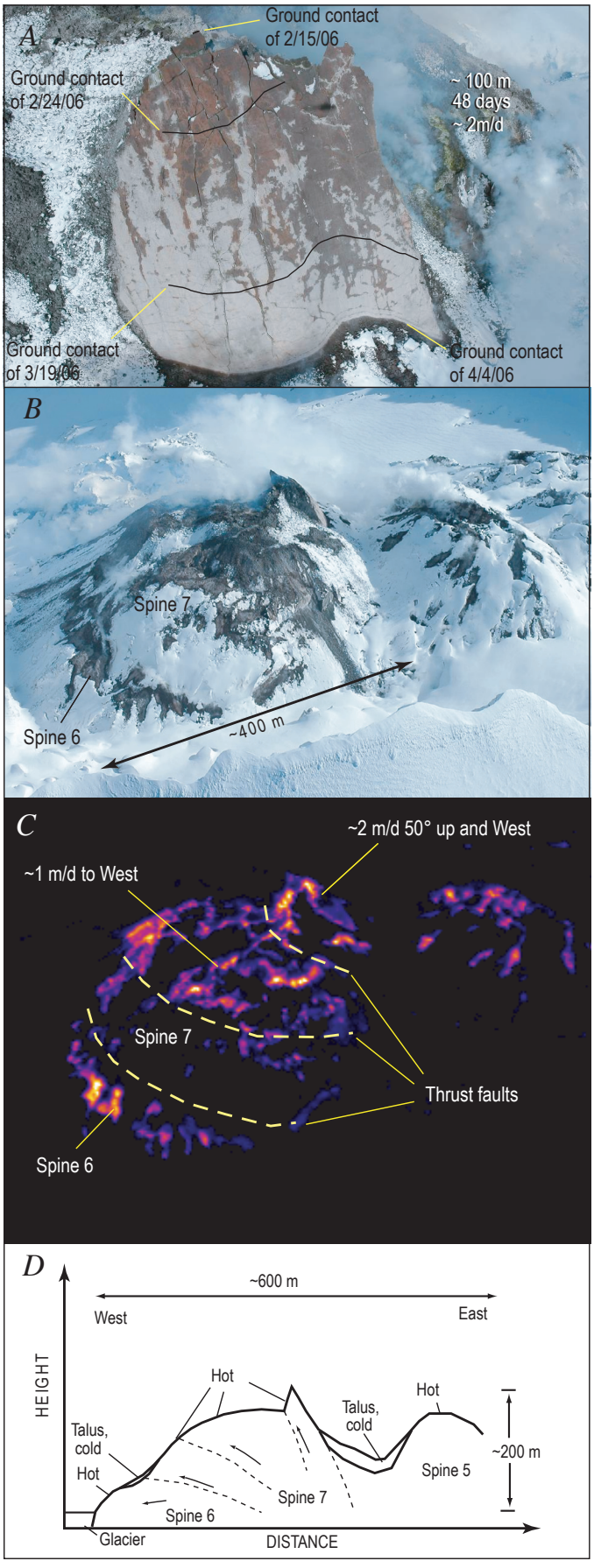

to the 30–40 m of excess elevation it had gained through uplift between August 2005 and February 2006 (fig. 21*A*).

Discussion

We consider here factors that influenced dome growth during the 2004–6 eruption. Potential near-surface controls on spine growth during the 2004–6 eruption include thick glacial ice, initial vent position and geometry, the 1986 topographic surface, and backpressure caused by spines pushing through and thrusting over debris from previous spines. We also consider the effects of dome growth on Crater Glacier. Lastly, we compare the 2004–6 Mount St. Helens dome-building eruption with well-documented historical examples at other volcanoes.

Effect of Glacier on Spine Growth

Glacier ice as thick as 150 m has apparently had little effect on the extrusion of the dome or on the growth of various spines, except to conceal substantial parts of them and to prevent shedding of disintegrating dome talus beneath the level of the glacier surface. As discussed in the introductory section, we infer that dome-glacier contacts have remained steep. Near-vertical contacts are consistent with ice-hot rock marginal boundaries observed at other locations. Examples include tuyas in British Columbia, Canada (Mathews, 1947), and ice-lava contacts at Mount Rainier (Lescinsky and Sisson, 1998). Glacial ice appeared not to impede spine growth significantly. Spines 2–4 grew recumbently to the south, pushing glacial ice aside as they progressed. Westward extension of spines 6 and 7 also pushed through thick glacial ice. The bed of the glacier was permeable enough that meltwater drained away without interacting with hot dome rock (Walder and others, this volume, chap. 13), except possibly during six brief phreatic explosions (Moran and others, this volume, chap. 6).

Vent Dimension and Location and Influence of 1980–86 Dome on Spine Growth

The depression from which the initial phreatic eruptions originated and from which the initial spine extruded was located at the west end of Opus and had an approximate

Figure 23. Photographs, thermal infrared image, and cross section of the Mount St. Helens crater on April 4, 2006. *A*, View looking west at 100-m fin showing previous ground-spine contacts. *B*, View looking northeast at spines 6 and 7. *C*, Thermal infrared image of view in *B*, looking northeast and showing thrust faults and relative motions. *D*, Schematic east-west cross section of growing spine 7, slowing spine 6, and stagnant spine 5. Orientation is roughly along line shown in *B* but extends east to spine 5. USGS photos by J.W. Vallance; thermal image by M. Logan.

Table 4. Timing, bearing, magnitude, and rate of deformation of one feature located on spine 6 at Mount St. Helens, Washington, between September 20, 2005, and February 9, 2006.

[Timing, direction, and magnitude of deformation are inferred from DEMs on given dates (Schilling and others, this volume, chap. 8).]

Interval	9/20/2005–10/24/2005	10/24/2005–12/15/2005	12/15/2005–2/9/2006
Days elapsed	34	52	56
Bearing	N80°W	N80°W	N85°W
Horizontal translation			
Displacement (m)	110	75	35
Rate (m/d)	3.2	1.4	0.6
Subsidence			
Displacement (m)	30	31	14
Rate (m/d)	0.9	0.6	0.3

diameter of 120 m (figs. 5, 12). Superimposing this vent location on the 1986 topographic surface (fig. 12) reveals that the initial vent was located on ice over the south-facing slope of the 1980–86 dome, in particular over the 1985 fault-formed ridge known as Opus. Just before the 2004 eruption, relief from the high point on Opus to the moat's floor beneath the glacier was ~130 m, and south-facing slopes were as steep as 40° under the trace of the vent (fig. 12).

The initial location of the 2004 vent, on steep south slopes of Opus, themselves buried beneath the glacier, clearly influenced the propensity of stiff spine extrusions to move southward. Several studies suggest that the magma ascending the conduit had largely solidified within a kilometer of the surface (Dzurisin and others, 2005; Iverson and others, 2006; and in this volume: Moran and others, chap. 2; Cashman and others, chap. 19; Pallister and others, chap. 30). We infer that, as the magma neared the surface in September 2004, the pre-existent solid plug of 1980–86 dome rock deflected the rising mass southward so that, near the surface, it tilted southward.

We tracked successive extrusion points at the surface by centering circles on the center of each spine origin with appropriate diameters equal to spine width (fig. 24). As the extrusion transitioned from the initial spine formation of phase 2 to well-developed whaleback-style spines of phase 3, the surface trace of the vent moved south and east. These trends continued until spine 3 began its breakup in December 2004. During the spine 3–4 transition this sense of movement reversed. However, during growth of spine 4, the southward and eastward motion recommenced. With extrusion of spine 5 during phase 4, the vent gradually moved westward back toward its original location. This motion increased with phase 5 extrusion of spine 6. With the onset of spine 7 extrusion, the surface manifestation of the vent returned to and remained within 20 m of its original position. Between vent clearing of phase 1 and initial whaleback-style intrusion of phase 3, the surface trace of the vent rapidly rose 130 m because an increasingly thick pile of lava built beneath it. Elevation of the vent trace increased slowly through extrusion of spines 4 and 5 during phases 3 and 4, then diminished with extension of spine 6 as phase 5 commenced. Extrusion of spine 7 rebuilt the lava pile beneath the vent, so that by early 2006 its trace was 200 m higher than its altitude in October 2004, though it was back to its original position in plan view.

Superimposing the position of the original vent and the seven spines on the 1986 surface suggests that the vent or conduit need not have shifted substantially at the depth of the initial erup-

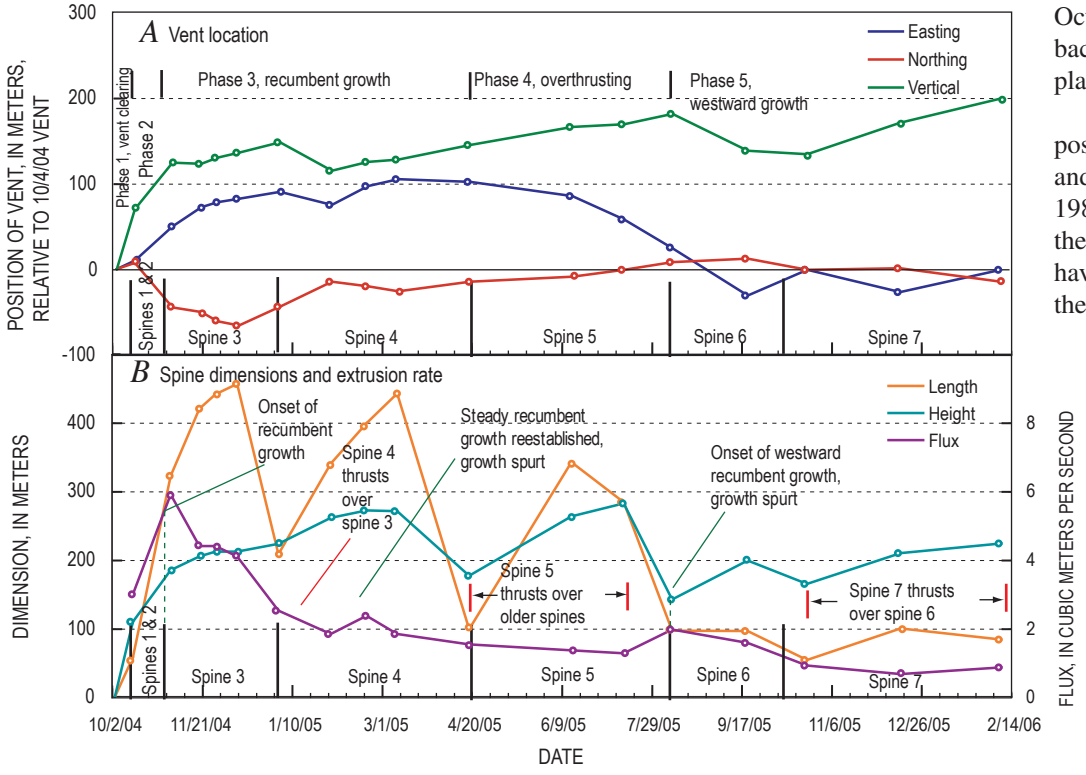

Figure 24. Plots of positions of vent, dimensions of spines, and extrusion flux versus time. *A*, Center of vent located in plan. *B*, Length of active spine, height of active spine, and lava discharge.

tion surface (figs. 12, 25). Geometry of the vent area permits origin of spines 1 through 4 from approximately the same initial vent location at the depth of the 1986 surface (fig. 12). Initially, extrusion of spines 1 and 2 covered the area directly above and to the south of the vent so that, as spine 3 began to grow upward and southward, previous spine and welt rubble diverted it eastward (fig. 12*A*). Additional dome rock and debris emplaced during spine 3 growth diverted spine 4 farther eastward. Eventually, so much dome rock had been pushed to the east that fragmented dome rock abutted the steep part of the east crater wall, and continuing spine extrusion could no longer push it aside. The subsequent spine (spine 5) therefore thrust instead over the older spines in a more southerly direction. When spine debris above the vent eventually built high enough, spine growth could extend westward across the rock debris of spines 1 and 2 (fig. 25). An inclined conduit did not simply increase in altitude; rather it shifted tens of meters southward, then south-southeastward, and finally southwestward as it evolved and grew higher (fig. 25). We suggest that vent geometry is such that spine extrusion throughout the eruption could have passed through approximately the same vent location at a depth near that of the 1986 surface and that migration of the vent's surface expression resulted from diversion by remnants of previous spines.

Influence of 1980–86 Surface on Spine Growth

Topography inherited from the 1980–86 eruption controlled growth patterns of the laterally propagating spines (figs. 12, 25). We superimposed the outlines of actively growing spines on topographic features concealed by glacier ice to assess their influence on growth patterns. Generally, we found that the 1986 topographic surface controlled recumbent

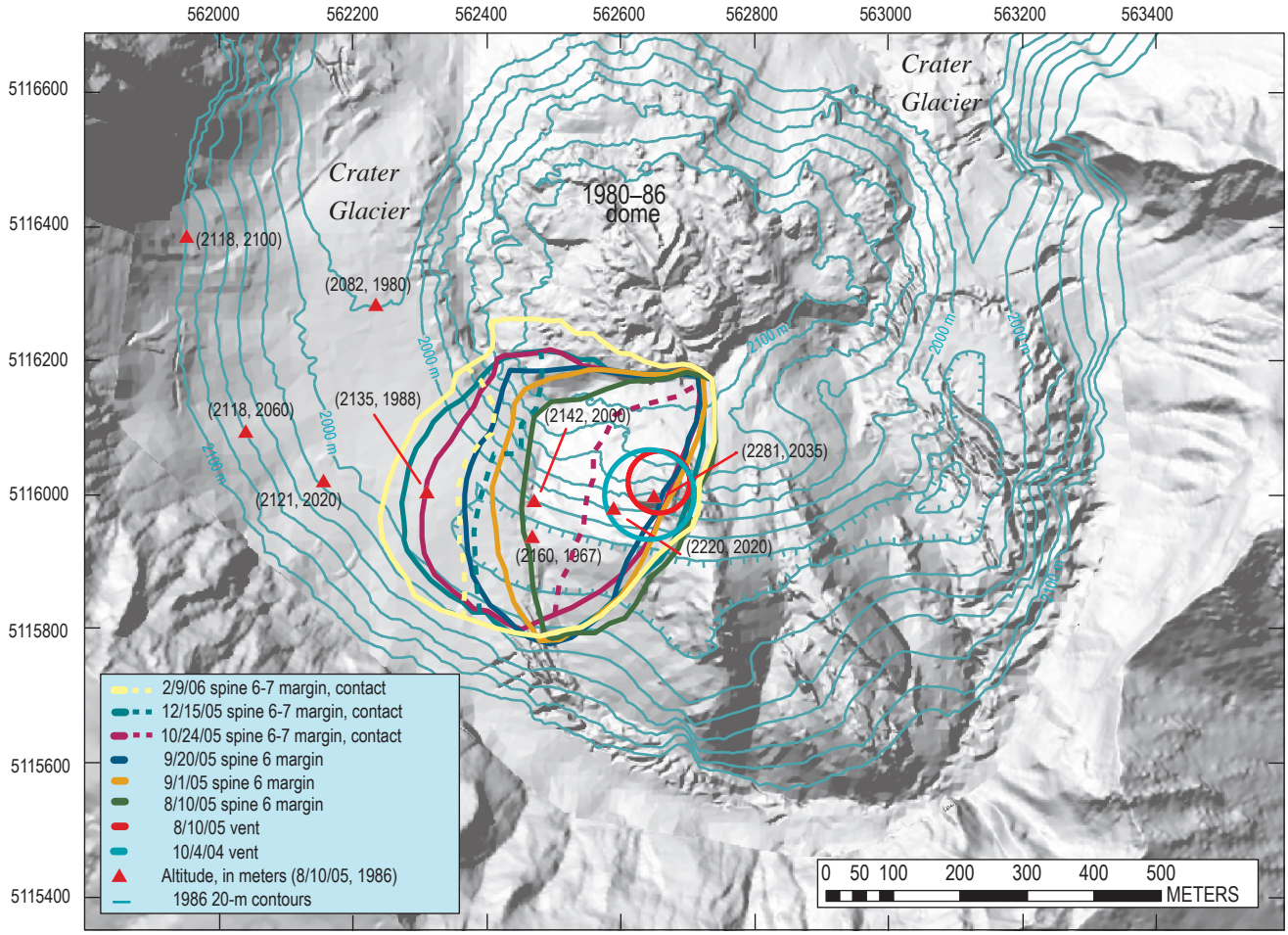

Figure 25. August 10, 2005, DEM showing outlines of spines 6 and 7 and their dome-glacier margins (solid lines) on dates indicated by colors in key. Dashed lines indicate contacts between spines 6 and 7 for appropriate dates indicated by colors in key. Select 20-m contours from 1986 DEM illustrate how composite spines 6 and 7 have migrated along a low topographic trough to west. Comparisons of altitudes on August 10, 2005, with those of 1986 are given for localities marked by red triangles.

growth directions, the rotation of spines, and how spines ultimately fragmented, but the ultimate barrier to continued lateral growth proved to be the walls of the 1980 crater modified by talus at their base and modified slightly by subsequent erosion.

After spine 1 grew, subsequent spines grew southward, in part because the crater floor sloped to the south. Spine 2 advanced due south until it encountered the steep opposing slopes of the south crater wall. Because spine 2 was then positioned directly south of the vent, the prominent whaleback of spine 3 that followed was forced slightly eastward as it advanced. Spine 3 extended across a broad basin to the south-southeast that was filled with glacial ice and welt debris. It then encountered the crater wall at an oblique angle (20°–30° from perpendicular) in mid-November 2004, and the influence of the wall deflected the snout of the spine eastward (fig. 12*A*). Once spine 4 had pushed remnants of its predecessor aside, it too progressed south-southeastward, encountered the 1980 crater wall at an oblique angle, and then rotated eastward (figs. 7, 15). A lack of such rotation before the spine arrived at buttressing slopes and fairly rapid rotation subsequently is strong evidence in support of the oblique-incidence hypothesis of rotation.

Both spines 3 and 4 began to fracture, crumble, and ultimately decouple from the source as a result of resistance to motion when they impinged on the crater wall. Spine 3 began to slow and break apart as it pushed against the crater walls in mid-November 2004. Two voluminous blocks and numerous smaller ones separated from the spine before it finally broke and fractured near its source on or about December 18, 2004. Thereafter, lava near the source slowly decoupled from remnants to the south to form spine 4. A similar sequence occurred when spine 4 itself met the wall, fractured at its root, and decoupled in April 2005 to form spine 5. In the April case, however, debris had filled the area east as far as the east crater wall, and thus spine 5 grew by southward thrusting across previous spine remnants.

Rotational motion of spines 3 and 4 in turn caused rotation of previously emplaced dome debris, welt debris, and glacier ice to the east. Southward spine propagation and oblique impingement on the crater wall apparently caused the rotation, and the less resistant expanse of glacial ice to the east permitted the rotation to proceed in that direction. By mid-April, when spine 4 and associated debris outboard of it had encountered steep slopes to the southeast as well as to the south, the counterclockwise rotation (map view) of phase 3 ceased (fig. 12*B*). Also at this time, the sense of rotation reversed from counterclockwise to clockwise, with a pivot 300 m south of the vent (fig. 19). The south end of spine 4 became fixed and the north end began to move east because the only available space east of the 2004–5 dome was located directly east of the vent (labeled "mid-April space east of vent" in fig. 12); no such space was available to the southeast.

Spine 5 thrust over remnants of spines 3 and 4 at steepening angles (fig. 18) until its perch atop those remnants became unstable. Failure along a north-south zone of weakness dipping steeply to the west allowed motion to resume along a 1986 topographic low, as spine 5 slumped together with westward growth of spine 6 (fig. 22). From April to August 2005, preexisting topography had little effect on spine growth because the active spine, 5, was shearing over previous spines rather than following old topographic surfaces. With extrusion of spine 6, westward spine migration pushed previous spine remnants and affiliated rubble westward into the topographic trough defined by the 1980–86 dome and the crater wall (fig. 25). This moat-like topography channeled growth of spine 6 such that it barely impinged on steeper slopes to the south and rode up on topographically high areas of the 1980–86 dome only near the vent, where some northward spreading and rockfall was underway. Similarly, as spine 7 thrust west into parts of spine 6, it pushed the earlier spine westward along the same topographic trough. As the volume of material to the west built, the rate of westward recession of the dome-glacier boundary slowed, and slabs of spine 7 extruded at steepening angles.

Extrinsic Control of Spine Growth Rate

An intrinsic exponential decline in overall extrusion rate (fig. 24) that probably derives from declining magma supply and pressurization is apparent during the course of the present eruption. Overprinted on this decline are several apparent increases in magma flux that may have been controlled extrinsically (spurts in fig. 24*B*). Time-averaged effusion rates commonly rise rapidly to a peak before falling slowly, resulting in an exponential decrease in eruption rate and declining growth (Harris and others, 2000). Such trends can be explained by the tapping of enclosed and pressurized magma chambers (Wadge, 1981; Harris and others, 2000). Extrinsic factors, such as changes in load, are thought to cause variation in effusion rates (Harris and others, 2003).

We hypothesized that increases or decreases in load near the surface might reduce or enhance extrusion rates, owing to increases and decreases in the mass displaced (fig. 24*B*). We plotted both relative height and length of active spines against time to test this idea. However, our results show no obvious correlation between spine length or height and extrusion rate (fig. 24*B*). A comparison between extrusion rate and style of extrusion suggests a possible correlation. Extrusion rate was greater when steady recumbent growth was established and smaller when active spines were thrusting upward at significant angles (fig. 24*B*). Steady lateral extrusion of spine 3 in late October and early November 2004 corresponded to an initial increase in discharge, and renewed steady extrusion of spine 4 in February 2005 corresponded to a slight increase in extrusion rate. A transition from thrusting to westward migration and slumping correlates to a third localized peak from late July to September 2005. Periods of resistance to movement caused by thrusting of spines at increasing angles over previous remnants also correlate with periods of diminished extrusion rate (fig. 24*B*). We suggest that such growth conditions may have acted to resist extrusion, suppressing the flux by backpressure. Slumping events and vent reorganization eased backpressure and thus enhanced flux.

Impact of Dome Growth on the Crater Glacier

Whereas the glacier had little affect on dome growth, spine growth did have a profound impact on the Crater Glacier—slicing it in two, pushing it hundreds of meters first one way then another, doubling it in thickness, but not melting it. As the response of Crater Glacier is the detailed subject of another contribution to this volume (Walder and others, chap. 13), we merely summarize the impact of spine growth on the glacier from the perspective of surface deformation vectors, which allowed us to track certain glacier features throughout nearly the entire course of the eruption. During October and November 2004, subsurface deformation owing to spine extrusion caused the glacier surface to take on first the appearance of a migrating wave of fractured ice and rock, then, with surfacing of spine 3 through that material, the appearance of bow waves of fractured snow and ice both west and east of the whaleback form. Once spine 3 divided the glacier in December 2004, it and its successor, spine 4, began slewing to the east, rotating about their tails and plowing the ice of the east glacier into a 100-m-high berm by January 2005. The berm then sluiced northward through the gap between the 1980–86 dome and the crater wall between April 2005 and February 2006 (fig. 26). Growth of spines 6 and 7, plus subsidence of dome remnants into west Crater Glacier, created a similar response between August and December 2005 whereby the glacier was first pushed up and westward (fig. 26) and then began to flow through the gap between the 1980–86 dome and crater wall. Despite its mistreatment, the glacier has lost no more than about 10 percent of its volume to contact melting as of February 2006 (Walder and others, this volume, chap. 13). Apparently, gouge-coated spines and shrouds of cold debris have effectively insulated glacier ice from hot spine interiors.

Comparison with Other Dome-Building Eruptions

Several factors set the 2004–6 dome-building eruption of Mount St. Helens apart from that of other well-documented historical domes such as those of Mount St. Helens 1980–86, Montserrat 1995–98, Santiaguito 1922–2006, and Unzen 1990–96. These include extrusion of solid spines, a propensity to form recumbent spines, interaction with glacier ice, and topographic setting. Mont Pelée in 1903 produced a spine that grew vertically but otherwise resembled whalebacks at Mount St. Helens. However, perhaps the historical dome-building eruption most similar to that of Mount St. Helens 2004–6 was the 1944–45 extrusion of the Showa-Shinzan dome at Usu volcano in Japan.

Mount St. Helens' 1980–86 dome extrusion differed from the present extrusion in extrusion rate, morphology, and process of emplacement. Excepting a one-year endogenous phase, extrusion of the 1980–86 dome occurred in discrete episodes, 16 of which were preceded by periods of accelerating endogenous growth, followed by extrusion of a viscous lobe, and terminated with periods of subsidence and lateral spreading (Swanson and Holcomb, 1990). In contrast, the present eruption has proceeded continuously with a general decline in discharge (fig. 24). Output of fresh dacite in the early phases of the present eruption occurred at a rate that is about one-half to one-third of rates measured during the 1980–86 episodes (Chadwick and others, 1988). The relentless growth during the 2004–6 eruption, however, has produced a total volume similar to that of the 1980–86 eruption in about one-fourth of the time.

Swanson and Holcomb (1990) document distinctive profiles for individual lobes emplaced during 1980–86, showing that lobes tended to adopt a characteristic slope (33°) and a characteristic height-to-diameter ratio (h/d) of about 0.32. The slope was approximately the angle of repose for coarse angular talus. In a more elaborate analysis, Iverson (1990) was able to model the characteristic slope in terms of a pressurized viscous magma enclosed by a brittle shell. Such a model is not applicable for spines of the present eruption because of the complicating influence of topographic barriers, glacial ice, and the subsolidus character of the magma, with the spines extruding in a near-solid state. Glacial ice within the crater has buttressed spines at slopes much greater than the angle of repose during the current eruption. Overall, the h/d ratio and slope for spines 3–7 ranged from 0.6 to 0.7 and from 50° to 60°, respectively. Those of initial spines were greater. Slopes higher than the angle of repose also reflect the massive and solid character of extruded spines. Such high h/d ratios are typical of upheaved domes and peléean spines (Blake, 1990).

Well-documented dome extrusion at Unzen, Japan, and Santiaguito, Guatemala, was continuous but varied in extru-

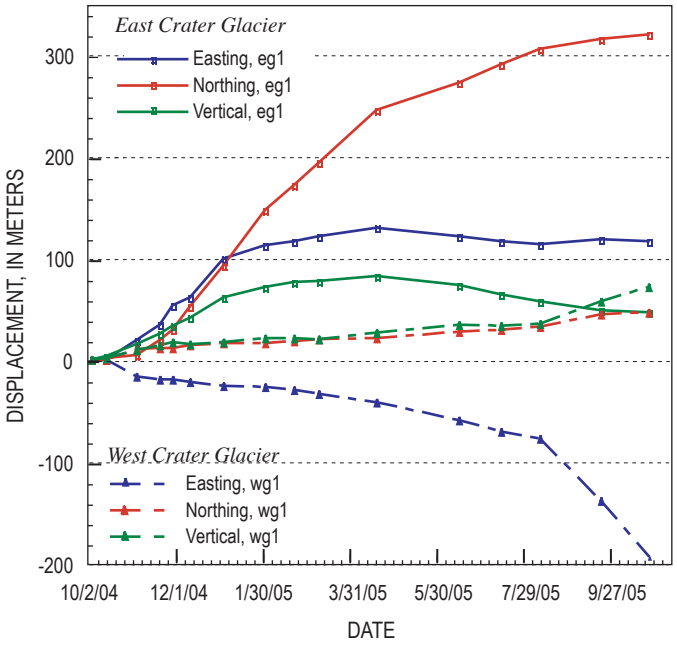

Figure 26. Displacement plots of a feature on east Crater Glacier (eg1 located at site a in fig. 2) and one on west Crater Glacier (wg1 located at site i in figs. 2*A*, 2*B*) versus time (both features are located at intervals in figs. 5, 7, 15, 19, 21).

sion rate and included both endogenous intrusion of viscous magma and extrusion of lava flows (Rose, 1980, 1987; Nakada and others, 1999; Harris and others, 2003). At Unzen, endogenous growth typified slow discharge, and exogenous growth typified more rapid discharge (Nakada and others, 1999). Over the course of the eruption, discharge slowed and endogenous growth increased proportionately (Nakada and others, 1999). Although Santiaguito has erupted continuously during 1922–2006, its growth has been episodic—waxing and waning over time scales of several years (Rose, 1987). In contrast to recent activity at Unzen, during Santiaguito's 84-year and ongoing eruption there has been a general tendency for the proportion of exogenous to endogenous growth to increase with time (Harris and others, 2003). Neither Unzen nor Santiaguito has shown the propensity to build solid-state spines at a low extrusion rate as observed during the current eruption at Mount St. Helens.

At Soufrière Hills volcano, Montserrat, Watts and others (2002) documented the morphology of lobes and spines, some of which superficially resemble those described here, and correlated them with extrusion rates. Watts and others (2002, their fig. 33) documented near-vertical spines, whaleback spines, and mega-spines that superficially resemble spines formed during the current eruption of Mount St. Helens, though similar forms here have had dimensions on a scale of hundreds of meters rather than tens of meters as observed at Soufrière Hills. With the exception of spine 1, the spines of the Mount St. Helens eruption have been larger and remained active longer than those at Soufrière Hills. Whaleback spines 3 and 4 grew during periods of months rather than days as at Montserrat, and spines 5 and 7 thrust over previous spines during periods of four months or more. The unusual, simultaneous slump and westward extrusion of spine 6 has no analogy to spine growth during any documented episode at Soufrière Hills volcano. More fluid morphologies, such as shear lobes and pancake lobes, did not occur during the Mount St. Helens 2004–6 eruption.

After its notorious eruption of 1902, Mont Pelée, Martinique, built a vertical spine that shares some characteristics with spines of the current Mount St. Helens eruption. That spine grew vertically to a height of more than 200 m in 1903 (Lacroix, 1904). Photographs (Lacroix, 1904) suggest that the spine was solid, had a gouge-coated and striated surface, and exposed a broken and massive surface on its opposite side. Like the Mount St. Helens spines, the Mont Pelée spine crumbled as it grew and eventually stagnated (Lacroix, 1904).

During its 1943–45 eruption, Showa-Shinzan dome of Mount Usu uplifted an area of as much as 1.5×1.5 km as much as 140 m (Mimatsu, 1995), generating a deformed zone reminiscent of the welt. Extrusion followed the deformation, as a jagged solid spine punched through the older roof rocks. As described by Mimatsu (1995), within nine days of initial unrest in December 1943, an area west of Mount Usu began to experience uplifting, folding, and faulting. Uplift to the west was initially strongest, after which its locus migrated in stages, eastward back toward the volcano. By June 1944, uplift ranged from 10 to 40 m. From June to November 1944, an additional 100 m of deformation accompanied 17 phreatic or phreatomagmatic explosions (Mimatsu, 1995). Finally, at the end of November 1944, the first lava spine pushed through the deformed and cratered uplifted area. Dacite spines continued to grow until August 1945. The spines commonly had a jagged appearance (Mimatsu, 1995), unlike those at Mount St. Helens. Like those at Mount St. Helens since 2004, the spines were completely solid on extrusion and showed no tendency to flow. The spines all rose more or less vertically, and none were described as having appreciable lateral components of motion (Mimatsu, 1995).

One spine at Mount Usu, Kobu-yama or Bump Mountain, did have a form more analogous to those of the present eruption of Mount St. Helens. Mimatsu (1995) describes it as having a shape like the bottom of a boat, with a coating of pulverized rock or dirt and grooves or scratches parallel to the direction of extrusion. The powdery surface is probably analogous to the gouge-coated surface of spines at Mount St. Helens. Mimatsu (1995) also described horizontal bands on Bump Mountain that were similar to the bands commonly observed on smooth surfaces of spines during 2004–6 at Mount St. Helens. The bands on Kobu-yama tended to form during periods of rain. Apparently, ash and debris that was constantly sloughing from the steep slopes of Kobu-yama stuck when the slopes were wetted. Furthermore, ash and debris accumulated at the base of the growing spine and stuck after heavy rains to form ledgelike bands that later rose as the spine extruded (Mimatsu, 1995). According to Mimatsu (1995), parts of these ledges were later shorn by falling debris.

Horizontal bands at Mount St. Helens are probably analogous, though not quite identical in origin, to those at Showa-Shinzan. Horizontal bands on spines at Mount St. Helens seem to have three forms, but all are plausibly related to moisture. The first, those most closely matching Mimatsu's (1995) description, are shelf-like accumulations of fine to coarse debris that stick to the smooth surfaces of spines at certain times, then rise with spine growth (fig. 27). At Mount St. Helens, these seem to correspond to stormy periods at the volcano. We suggest that, as at Showa-Shinzan, addition of water to mixtures of fine and coarse debris immediately adjacent to the hot base of the extruding spine creates a weak cement that subsequently dries against the hot spine. A variation on this process involves only the fine-grained ash at the base of the spine and requires relatively less moisture. These bands are much less prominent. Photographs show fine debris concentrated at the base of the spines (fig. 27). This material requires less water to form a cement and, hence less moisture is required to create horizontal bands of such fine ash. A third, most common but least prominent variety of band, appears to involve periodic darkening of the gouge-coated surface. No one has examined these closely enough to understand if there is an accumulation of material associated with them or if they are merely stains. We speculate that many of them are related to nightly dew. All of these bands are fragile and ephemeral.

Conclusions

Spine extrusion and associated near-vent deformation at Mount St. Helens during 2004–6 presented an opportunity to test and apply various methods to track, measure, and characterize the dynamics and morphologies of extrusion and nearby deformation during a dome-forming eruption. We summarize here our chief conclusions drawn from our data and the methodology that generated it.

Thermal infrared (TIR) surveys proved useful in differentiating events and structures that were cold from those that were hot. The TIR surveys showed that the explosions of October 1–5 were phreatic rather than magmatic. Imagery from TIR surveys also proved useful in identifying areas where spines were about to emerge. These were apparent as broad areas that warmed substantially in the days immediately prior to extrusion. Once spines began extruding, regular TIR surveys helped document their growth, character, and structures within them. Finally, TIR images helped monitoring crews identify places on

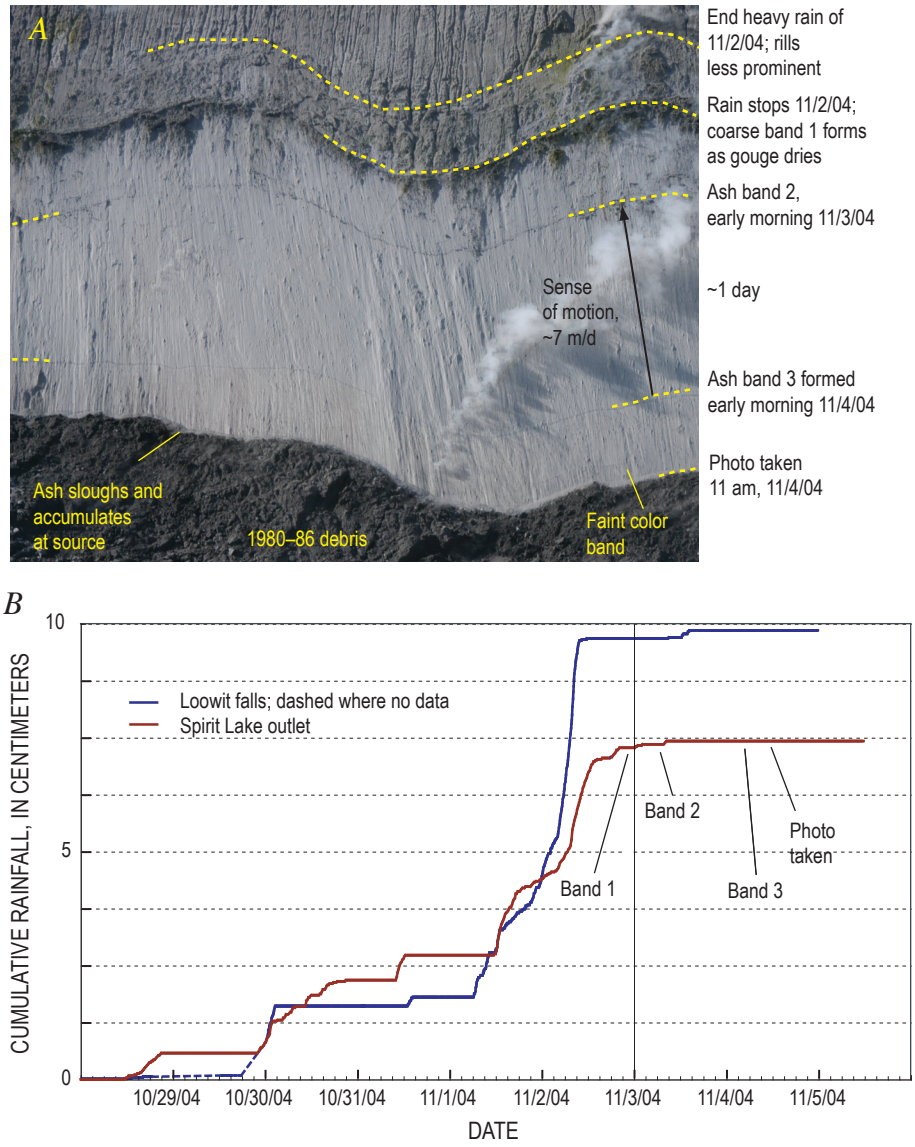

Figure 27. Photograph of emerging spine and plot of rainfall from October–November 2004. *A*, Close-up view of spine 3 east flank at 11 a.m. on November 4, 2004. Coarse band 1 consists of mixtures of ash and coarse lithic lapilli, more subtle bands 2 and 3 consist of ash, and very faint ones may be stains. Band formation is associated with increases in moisture. USGS photo by J.S. Pallister. *B*, Cumulative rainfall versus time from USGS gages at Loowit falls (crater mouth) and at Spirit Lake outlet and time of emergence of notable bands. Rainfall data courtesy of K. Spicer, USGS.

the dome cool enough to place GPS instruments and accelerometers (Schneider and others, this volume, chap. 17).

Data collected as part of this study along with others in this volume suggest solid-state extrusion throughout the current dome-building episode. TIR measurement of deep cracks and newly exposed surfaces give temperatures well below the solidus of the dacite magma being erupted. Morphology of the various spines exhibits no flowage features like lobes, coulees, or ramp structures. Indeed, yield strength has apparently been so high that the spines can stand at steep slopes until they crumble. New spines have typically formed as previous ones have undergone brittle failure and fracturing, then shearing off to form stagnant crumbling masses.

Tracking of features in successive sets of aerial photographs and DEMs has enabled the development of surface-deformation vector fields during 17 time intervals, which have varied in duration from 1 to 55 days. Each vector field gives a comprehensive spatial sense of deformation during that interval. Each also indicates the nature of advance or motion during the interval. Time-lapse photography and GPS instruments provided extra detail on much finer time scales for specific localities and localized fields of view, but the DEM tracking provided a valuable synoptic perspective.

Chief near-surface controls on spine extrusion during the 2004–6 eruption have been vent location, relict surfaces such as the 1980 crater structure and the 1980–86 dome, and spine remnants emplaced during previous phases of the present eruption—but not glacial ice. Ice as thick as 150 m has obscured eruptive processes, prevented formation of marginal angle-of-repose talus fans, and encouraged steep boundary slopes to the new dome complex through buttressing, but it has not significantly impeded spines pushing through it. Spines initially emerged at a location over the steep south-facing slope of the 1980–86 dome, which dictated their initial southward propagation. The glacier-filled space of the moat between the 1980 crater walls and the 1980–86 dome permitted southward propagation of spines 2 to 4 and funneled spines 6 and 7 westward. Spine 2 impinged on the opposing slope of the crater and stopped. In contrast, recumbent whaleback spines 3 and 4 impinged at oblique angles and rotated eastward before cracking up. Although the vent location at the 2004–6 surface shifted east and south more than 100 m before moving back to the west, its altitude increased ~200 m due to piling up of lava over the initial vent. The vent position relative to its initial trace at the 1986 surface need not have moved substantially. Once spine remnants occupied all available open space to the south, new spines thrust over previous remnants. Resistance to extrusion during intense periods of thrusting may have slowed extrusion rates because of backpressure effects during certain time intervals.

Although Crater Glacier had minimal influence on the growing spines, spine growth affected the glacier dramatically, initially dividing it into two arms and then bulldozing it hundreds of meters first east (east arm), then west (west arm), while heaping it more than 100 m higher than its original altitude.

The 2004–6 eruption has thus far differed from other well-documented historical eruptions in its solid-state character, its recumbent growth style, and its interaction with the glacier. On the basis of historical records, most domes grow endogenously; exogenously to produce thick units with a high aspect ratio and, sometimes, longer lava flows; or a combination of both (Blake, 1990). Peléean spines like those at Mont Pelée or Soufrière Hills are similar to those of the current eruption, but the 1943–45 eruption of Mount Usu provides the closest historical analogue. Perhaps the most similar of historically documented domes are those sometimes referred to as upheaved plugs (Blake, 1990). Such plugs appear to push up bodily like pistons and, when they reach the surface, have sufficient strength not to deform or spread outward but instead ascend vertically. Mimatsu (1995) beautifully documents the evolution of one such upheaval dome from 1943 to 1945 at Mount Usu in Japan. The intriguing variations in pluglike dome construction and evolution at Mount St. Helens since 2004, not previously well documented, have been recumbent growth and interaction with an unusual combination of topographic constraints and glacial ice.

Acknowledgments

We thank Andy Harris and Michelle Coombs for careful reviews of this manuscript. Andy's very detailed comments, in particular, greatly improved the paper. Cascades Volcano Observatory staff were generous with their time, their ideas, and their data.

References Cited

Ball, M., and Pinkerton, H., 2006, Factors affecting the accuracy of thermal imaging cameras in volcanology: Journal of Geophysical Research, v. 111, no. B11, B11203, doi.10.1029/2005Jb003829, 14 p.

Blake, S., 1990, Viscoplastic models of lava domes, *in* Fink, J.H., ed., Lava flows and domes, emplacement mechanisms and hazard implications: Berlin, Springer-Verlag, International Association of Volcanology and Chemistry of the Earth's Interior, Proceedings in Volcanology 2, p. 89–126.

Cashman, K.V., Thornber, C.R., and Pallister, J.S., 2008, From dome to dust; shallow crystallization and fragmentation of conduit magma during the 2004–2006 dome extrusion of Mount St. Helens, Washington, chap. 19 *of* Sherrod, D.R., Scott, W.E., and Stauffer, P.H., eds., A volcano rekindled; the renewed eruption of Mount St. Helens, 2004–2006: U.S. Geological Survey Professional Paper 1750 (this volume).

Chadwick, W.W., Archuleta, R.J., and Swanson, D.A., 1988, The mechanics of ground deformation precursory to dome-

building extrusions at Mount St. Helens 1981–1982: Journal of Geophysical Research, v. 93, no. B5, p. 4351–4366, doi:10.1029/88JB01345.

Dzurisin, D., Vallance, J.W., Gerlach, T.M., Moran, S.C., and Malone, S.D., 2005, Mount St. Helens reawakens: Eos (American Geophysical Union Transactions), v. 86, no. 3, p. 25, 29.

Dzurisin, D., Lisowski, M., Poland, M.P., Sherrod, D.R., and LaHusen, R.G., 2008, Constraints and conundrums resulting from ground-deformation measurements made during the 2004–2005 dome-building eruption of Mount St. Helens, Washington, chap. 14 *of* Sherrod, D.R., Scott, W.E., and Stauffer, P.H., eds., A volcano rekindled; the renewed eruption of Mount St. Helens, 2004–2006: U.S. Geological Survey Professional Paper 1750 (this volume).

Gerlach, T.M., McGee, K.A., and Doukas, M.P., 2008, Emission rates of CO_2, SO_2, and H_2S, scrubbing, and preeruption excess volatiles at Mount St. Helens, 2004–2005, chap. 26 *of* Sherrod, D.R., Scott, W.E., and Stauffer, P.H., eds., A volcano rekindled; the renewed eruption of Mount St. Helens, 2004–2006: U.S. Geological Survey Professional Paper 1750 (this volume).

Harris, A.J.L., Murray, J.B., Aries, S.E., Davies, M.A., Flynn, L.P., Wooster, M.J., Wright, R., and Rothery, D.A., 2000, Effusion rate trends at Etna and Krafla and their implications for eruptive mechanisms: Journal of Volcanology and Geothermal Research, v. 102, p. 237–270.

Harris, A.J.L., Flynn, L.P., Matías, O., and Rose, W.I., 2002, The thermal stealth flows of Santiaguito dome, Guatemala: Implications for the cooling and emplacement of dacitic block-lava flows: Geological Society of America Bulletin, v. 114, no. 5, p. 533–546.

Harris, A.J.L., Rose, W.I., and Flynn, L.P., 2003, Temporal trends in lava dome extrusion at Santiaguito 1922–2000: Bulletin of Volcanology, v. 65, p. 77–89.

Harris, A.J.L., Flynn, L.P., Matías, O., Rose, W.I., and Cornejo, J., 2004, The evolution of an active lava flow field: an ETM+ perspective: Journal of Volcanology and Geothermal Research, v. 135, p. 147–168.

Harris, A.J.L., Dehn, J., Patrick, M.R., Calvari, S., Ripepe, M., and Lodato, L., 2005, Lava effusion rates from hand-held thermal infrared imagery; an example from the June 2003 effusive activity at Stromboli: Bulletin of Volcanology, v. 68, no. 2, p. 107–117.

Herriott, T.M., Sherrod, D.R., Pallister, J.S., and Vallance, J.W., 2008, Photogeologic maps of the 2004–2005 Mount St. Helens eruption, chap. 10 *of* Sherrod, D.R., Scott, W.E., and Stauffer, P.H., eds., A volcano rekindled; the renewed eruption of Mount St. Helens, 2004–2006: U.S. Geological Survey Professional Paper 1750 (this volume).

Iverson, R.M., 1990, Lava domes modeled as brittle shells that enclose pressurized magma, with application to Mount St. Helens, *in* Fink, J.H., ed., Lava flows and domes, emplacement mechanisms and hazard implications: Berlin, Springer-Verlag, International Association of Volcanology and Chemistry of the Earth's Interior, Proceedings in Volcanology 2, p. 47–69.

Iverson, R.M., Dzurisin, D., Gardner, C.A., Gerlach, T.M., LaHusen, R.G., Lisowski, M., Major, J.J., Malone, S.D., Messerich, J.A., Moran, S.C., Pallister, J.S., Qamar, A.I., Schilling, S.P., and Vallance, J.W., 2006, Dynamics of seismogenic volcanic extrusion at Mount St. Helens in 2004–05: Nature, v. 444, no. 7118, p. 439–443, doi:10.1038/nature05322, supplementary movie 2 at http://www.nature.com/nature/journal/v444/n7118/suppinfo/nature05322.html.

Lacroix, A., 1904, La Montagne Pelée et ses eruptions: Paris, Maison et Cie, 662 p.

LaHusen, R.G., Swinford, K.J., Logan, M., and Lisowski, M., 2008, Instrumentation in remote and dangerous settings; examples using data from GPS "spider" deployments during the 2004–2005 eruption of Mount St. Helens, Washington, chap. 16 *of* Sherrod, D.R., Scott, W.E., and Stauffer, P.H., eds., A volcano rekindled; the renewed eruption of Mount St. Helens, 2004–2006: U.S. Geological Survey Professional Paper 1750 (this volume).

Lescinsky, D.T., and Sisson, T.W., 1998, Ridge-forming, ice-bounded lava flows at Mount Rainier, Washington: Geology, v. 26, p. 943–946.

Major, J.J., Kingsbury, C.G., Poland, M.P., and LaHusen, R.G., 2008, Extrusion rate of the Mount St. Helens lava dome estimated from terrestrial imagery, November 2004–December 2005, chap. 12 *of* Sherrod, D.R., Scott, W.E., and Stauffer, P.H., eds., A volcano rekindled; the renewed eruption of Mount St. Helens, 2004–2006: U.S. Geological Survey Professional Paper 1750 (this volume).

Mathews, W.H., 1947, "Tuyas"; flat topped volcanoes in northern British Columbia: American Journal of Science, v. 245, p. 560–570.

Mimatsu, M., 1995, Showa-Shinzan diary, expanded reprint: Sapporo, Suda Seihan Co., 179 p.

Moran, S.C., Malone, S.D., Qamar, A.I., Thelen, W.A., Wright, A.K., and Caplan-Auerbach, J., 2008a, Seismicity associated with renewed dome building at Mount St. Helens, 2004–2005, chap. 2 *of* Sherrod, D.R., Scott, W.E., and Stauffer, P.H., eds., A volcano rekindled; the renewed eruption of Mount St. Helens, 2004–2006: U.S. Geological Survey Professional Paper 1750 (this volume).

Moran, S.C., McChesney, P.J., and Lockhart, A.B., 2008b, Seismicity and infrasound associated with explosions at Mount St. Helens, 2004–2005, chap. 6 *of* Sherrod, D.R.,

Scott, W.E., and Stauffer, P.H., eds., A volcano rekindled; the renewed eruption of Mount St. Helens, 2004–2006: U.S. Geological Survey Professional Paper 1750 (this volume).

Nakada, S., Shimizu, H., and Ohta, K., 1999, Overview of the 1990–1995 eruption at Unzen Volcano: Journal of Volcanology and Geothermal Research, v. 89, nos. 1–4, p. 1–22, doi:10.1016/S0377-0273(98)00118-8.

Pallister, J.S., Thornber, C.R., Cashman, K.V., Clynne, M.A., Lowers, H.A., Mandeville, C.W., Brownfield, I.K., and Meeker, G.P., 2008, Petrology of the 2004–2006 Mount St. Helens lava dome—implications for magmatic plumbing and eruption triggering, chap. 30 *of* Sherrod, D.R., Scott, W.E., and Stauffer, P.H., eds., A volcano rekindled; the renewed eruption of Mount St. Helens, 2004–2006: U.S. Geological Survey Professional Paper 1750 (this volume).

Poland, M.P., Dzurisin, D., LaHusen, R.G., Major, J.J., Lapcewich, D., Endo, E.T., Gooding, D.J., Schilling, S.P., and Janda, C.G., 2008, Remote camera observations of lava dome growth at Mount St. Helens, Washington, October 2004 to February 2006, chap. 11 *of* Sherrod, D.R., Scott, W.E., and Stauffer, P.H., eds., A volcano rekindled; the renewed eruption of Mount St. Helens, 2004–2006: U.S. Geological Survey Professional Paper 1750 (this volume).

Queija, V.R., Stoker, J.M., and Kosovich, J.J., 2005, Recent U.S. Geological Survey applications of Lidar: Photogrammetric Engineering and Remote Sensing, v. 71, no. 1, p. 5–9.

Rose, W.I., 1980, The geology of Santiaguito volcanic dome Guatemala: Hanover, N.H., Dartmouth College, Ph.D. dissertation, 253 p.

Rose, W.I., 1987, Volcanic activity at Santiaguito volcano, 1976–1984, *in* Fink, J.H., ed., The emplacement of silicic domes and lava flows: Geological Society of America Special Paper 212, p. 17–27.

Schilling, S.P., Carrara, P.E., Thompson, R.A., and Iwatsubo, E.Y., 2004, Posteruption glacier development within the crater of Mount St. Helens, Washington, USA: Quaternary Research, v. 61, no. 3, p. 325–329.

Schilling, S.P., Thompson, R.A., Messerich, J.A., and Iwatsubo, E.Y., 2008, Use of digital aerophotogrammetry to determine rates of lava dome growth, Mount St. Helens, Washington, 2004–2005, chap. 8 *of* Sherrod, D.R., Scott, W.E., and Stauffer, P.H., eds., A volcano rekindled; the renewed eruption of Mount St. Helens, 2004–2006: U.S. Geological Survey Professional Paper 1750 (this volume).

Schneider, D.J., Vallance, J.W., Wessels, R.L., Logan, M., and Ramsey, M.S., 2008, Use of thermal infrared imaging for monitoring renewed dome growth at Mount St. Helens, 2004, chap. 17 *of* Sherrod, D.R., Scott, W.E., and Stauffer, P.H., eds., A volcano rekindled; the renewed eruption of Mount St. Helens, 2004–2006: U.S. Geological Survey Professional Paper 1750 (this volume).

Swanson, D.A., and Holcomb, R.T., 1990, Regularities in growth of the Mount St. Helens dacite dome, 1980–1986, *in* Fink, J.H., ed., Lava flows and domes, emplacement mechanisms and hazard implications: Berlin, Springer-Verlag, International Association of Volcanology and Chemistry of the Earth's Interior, Proceedings in Volcanology 2, p. 3–24.

Thelen, W.A., Crosson, R.S., and Creager, K.C., 2008, Absolute and relative locations of earthquakes at Mount St. Helens, Washington, using continuous data; implications for magmatic processes, chap. 4 *of* Sherrod, D.R., Scott, W.E., and Stauffer, P.H., eds., A volcano rekindled; the renewed eruption of Mount St. Helens, 2004–2006: U.S. Geological Survey Professional Paper 1750 (this volume).

Turcotte, D.L., and Schubert, G., 1982, Geodynamics: New York, John Wiley, 450 p.

Wadge, G., 1981, The variation of magma discharge during basaltic eruptions: Journal of Volcanology and Geothermal Research, v. 11, p. 139–168.

Walder, J.S., Schilling, S.P., Vallance, J.W., and LaHusen, R.G., 2008, Effects of lava-dome growth on the Crater Glacier of Mount St. Helens, Washington, chap. 13 *of* Sherrod, D.R., Scott, W.E., and Stauffer, P.H., eds., A volcano rekindled; the renewed eruption of Mount St. Helens, 2004–2006: U.S. Geological Survey Professional Paper 1750 (this volume).

Watts, R.B., Herd, R.A., Sparks, R.S.J., and Young, S.R., 2002, Growth patterns and emplacement of the andesitic lava dome at Soufrière Hills Volcano, Montserrat, *in* Druitt, T.H., and Kokelaar, B.P., eds., The eruption of Soufrière Hills Volcano, Montserrat from 1995 to 1999: Geological Society of London Memoir 21, p. 115–152.